J. Fluid Mech. (1979), *vol.* 92, *part* 2, *pp.* 349–379
Printed in Great Britain

The spectral energy transfer from surface waves to internal waves

By DIRK J. OLBERS

Institut für Geophysik, Universität Hamburg, and Max-Planck-Institut für Meteorologie, Hamburg, Germany†

AND KLAUS HERTERICH

Max-Planck Institut für Meteorologie, Hamburg, Germany

(Received 30 September 1977)

The generation of internal waves by resonantly interacting surface waves is examined in the framework of spectral scattering theory in the random-phase approximation. Coupling coefficients are derived from Euler's equation of motion for arbitrary stratification. The spectral energy transfer is discussed for deep-water surface waves and a simple three-layer model of the stability frequency. Analytical and numerical evaluation of the transfer integral leads to a parametrization in terms of the basic model parameters. These are the depth, thickness and stability frequency of the thermocline and the scale parameters and bandwidth of the surface wave spectrum. Strong dependence on some of these parameters, in particular the surface wave energy and the ratio of surface and internal wave frequencies, indicates a large spatial and temporal variability of the transfer rate. The transfer to the internal wave field in the oceanic main thermocline is found to be negligible compared with the effect of other processes. High frequency waves in the seasonal thermocline may be generated very efficiently.

1. Introduction

Internal waves may be generated by resonant interaction of pairs of surface gravity waves. This process has been investigated experimentally and theoretically with the aim of establishing its relevance in the ocean. The coupling between standing surface and internal waves in a tank has been studied by Joyce (1974), for example. Theoretical models of the interaction between discrete waves have been developed by Ball (1964), Thorpe (1966), Nesterov (1972), Brekhovskikh *et al.* (1972) and others. These authors represent the interacting surface waves as infinitely coherent, sinusoidal waves with deterministic phase relations. Although these models are useful for clarifying the dynamics and for demonstrating the possible occurrence of the process, the application of the results to the ocean is limited.

An attempt to estimate the spectral growth of the oceanic internal wave field within the framework of deterministic wave components was recently made by Watson, West & Cohen (1976). To model the energy transfer from an equilibrium surface wave spectrum these authors represent the spectrum by a large but finite set of wave components and numerically integrate the time behaviour of all amplitudes and phases involved in the interaction. This model may be applicable to a sea state which

† Present address: Institut für Meereskunde, Universität Kiel, Germany.

0022–1120/79/4029–6460 $02.00

shows a regular pattern for long times (compared with the interaction time). Even for long-wavelength swell where the wave motion can be discerned for some wavelengths, this constraint is only marginally satisfied and the adequacy of the model is questionable. In other situations such as the case of wind–sea, when the ocean surface wave field shows a random pattern, its spectrum is better modelled by a large (in fact a continuous) ensemble of stochastic wave trains than by a superposition of deterministic waves. In the case of a continuous spectrum a wave (as a narrow-band superposition of Fourier components) can be identified only for times small compared with the spectral bandwidth associated with it. For longer times its identity is lost owing to phase-mixing of the spectral components by which it has been supported. This is the kind of model which we shall pursue in this paper. It inherently yields smaller growth rates, since because of phase-mixing the interacting wave components will change their phase relations and go out of resonance much faster than in a deterministic model where phases change only as a consequence of the mode coupling.

Generation of internal waves by surface waves is one of the few processes for which the modification of the internal wave spectrum can be discussed at present because surface wave spectra are known and thus the input function can be computed. In his general theory of geophysical nonlinear interactions Hasselmann (1966, 1967) derived a spectral transfer equation which adequately describes the interaction of waves in random wave fields. This concept was pursued by Kenyon (1968), who determined the energy transfer from an observed swell spectrum to the first internal wave mode in shallow water. Using a constant stability-frequency stratification, he came to the conclusion that the observed level of internal wave fluctuations could not have been generated by the observed swell. Joyce (1974) pointed out that this conclusion must be reconsidered using more realistic models of the stratification because the coupling strongly depends on the overlapping of surface and internal wave modes.

The relevance of the process for the oceanic internal wave field is thus still unclear. We discuss the spectral transfer from the surface to the internal wave field in the framework of Hasselmann's transfer equation. Though the interaction coefficients are derived for the general case, the further analysis is restricted to surface waves in a deep ocean. A simple three-layer model of the stability frequency is used which represents either the oceanic main thermocline or a seasonal thermocline. The spectral transfer rates are computed by analytical and numerical means to derive a parametrization in terms of the basic model parameters. These are the thermocline depth and thickness, the maximum stability frequency in the thermocline, and the scale parameters and bandwidth of the surface wave spectrum. Details of the shape of the spectrum turn out to be of minor importance with the exception of the spectral widths of the distributions of wavenumber and wave-direction.

The parametrization of the transfer rate reveals a strong dependence on some of the model parameters, in particular the frequency ratio of surface and internal waves and the surface wave energy. Since these quantities show a large temporal and spatial variability in the ocean the magnitude of the transfer changes by some orders of magnitude for different oceanic parameter ranges. Nevertheless we may conclude the process has no influence at all, even under extreme conditions, on the universal equilibrium internal wave field in the main thermocline. Owing to the stronger stratification and the resulting smaller frequency gap between surface and internal waves the process is far more effective in the seasonal thermocline. It may be of significant

importance for the waves trapped in the seasonal thermocline. We expect that the interaction can be identified in high frequency data of the upper ocean because of the strong parametric dependence and outstanding directional distribution of the transfer rate.

In §2 we derive the response in the internal wave modes to arbitrary forcing. Section 3 and appendix A present the forcing function of resonantly interacting wave components and introduce the spectral transfer equation describing the spectral energy flux from the surface wave field to the internal wave modes. In §4 we discuss the transfer for a deep ocean. Section 5 constitutes a summary of the results.

2. The internal wave response to arbitrary forcing

The ocean will be described as an incompressible, stratified, rotating fluid of infinite horizontal extent. We shall use Cartesian co-ordinates $(x_1, x_2, x_3 = z)$ with the x_3 axis pointing vertically upwards. We separate the density and pressure fields into the mean equilibrium fields $\bar{\rho}(x_3)$ and $\bar{p}(x_3)$, related by

$$d\bar{p}/dx_3 = -g\bar{\rho}, \tag{2.1}$$

and the deviations $\rho(x_j, t)$ and $p(x_j, t)$. The equations of motion then take the form†

$$\left.\begin{aligned} \bar{\rho}\{\partial_t u_i + \epsilon_{ijk} f_j u_k\} + g_i \rho + \partial_i p = S_i \quad (i = 1, 2, 3), \\ \partial_t \rho + u_3 d\bar{\rho}/dx_3 = S_4, \\ \partial_i u_i = 0, \end{aligned}\right\} \tag{2.2}$$

where $f_j = \delta_{j3} f$ and $g_j = \delta_{j3} g$. The nonlinear terms have been collected on the right-hand side by defining

$$\left.\begin{aligned} S_i = -\bar{\rho} u_j \partial_j u_i - \rho\{\partial_t u_i + \epsilon_{ijk} f_j u_k\} \quad (i = 1, 2, 3), \\ S_4 = -u_j \partial_j \rho. \end{aligned}\right\} \tag{2.3}$$

At the free surface $x_3 = \zeta(x_\alpha, t)$ the kinematical and dynamical boundary conditions

$$\partial_t \zeta + u_\alpha \partial_\alpha \zeta - u_3 = 0, \quad p + \bar{p} = 0 \tag{2.4}$$

are to be satisfied. The atmospheric pressure has been included in $\bar{p}$. By expansion about the undisturbed free surface $x_3 = 0$ the nonlinear terms in (2.4) may be separated. We find

$$\left.\begin{aligned} \partial_t \zeta - u_3 = S_5 \\ p - \bar{\rho} g \zeta = S_6 \end{aligned}\right\} \quad \text{at} \quad x_3 = 0, \tag{2.5}$$

with

$$\left.\begin{aligned} S_5 = \zeta \partial_3 u_3 - u_\alpha \partial_\alpha \zeta + \ldots, \\ S_6 = \tfrac{1}{2} \zeta^2 g\, d\bar{\rho}/dx_3 - \zeta \partial_3 p + \ldots, \end{aligned}\right\} \tag{2.6}$$

correct to second order in the field components.

At the bottom $x_3 = -H + h(x_\alpha)$ the boundary condition

$$u_3 - u_\alpha \partial_\alpha h = 0 \tag{2.7}$$

† Latin indices $i, j, k = 1, 2, 3$, Greek indices $\alpha, \beta = 1, 2$. $\epsilon_{ijk} = 1(-1)$ if (i, j, k) is an even (odd) permutation of $(1, 2, 3)$, $\epsilon_{ijk} = 0$ otherwise. $\epsilon_{\alpha\beta} = 1(-1)$ if (α, β) is an even (odd) permutation of $(1, 2)$, $\epsilon_{\alpha\beta} = 0$ otherwise.

states the vanishing of the normal velocity. If we expand (2.7) about the mean water depth $x_3 = -H$ we obtain

$$u_3 = S_7 \quad \text{at} \quad x_3 = -H \tag{2.8}$$

with

$$S_7 = u_\alpha \partial_\alpha h - h\partial_3 u_3 - \tfrac{1}{2}h^2 \partial_3^2 u_3 + h\partial_3(u_\alpha \partial_\alpha h) + \ldots, \tag{2.9}$$

correct to $O(h^2)$.

The equations of motion and boundary conditions can be reduced by standard manipulations to

$$\mathscr{L}[u_3] = \bar{\rho}^{-1}\partial_3 \bar{\rho}\, \partial_3[\partial_t^2 + f^2]\, u_3 + \partial_\alpha^2[\partial_t^2 + N^2]\, u_3 = Q_1, \tag{2.10}$$

with the boundary conditions

$$\left.\begin{aligned} [\partial_t^2 + f^2]\, \partial_3 u_3 - g\partial_\alpha^2 u_3 &= Q_2 \quad \text{at} \quad x_3 = 0, \\ u_3 &= Q_3 \quad \text{at} \quad x_3 = -H. \end{aligned}\right\} \tag{2.11}$$

We have introduced

$$N(x_3) = \left(-\frac{g}{\bar{\rho}}\frac{d\bar{\rho}}{dx_3}\right)^{\frac{1}{2}}, \tag{2.12}$$

which is the stability frequency associated with the basic stratification, which we assume to be stable. The forcing functions Q_1, Q_2 and Q_3 can be expressed in terms of the S_j as

$$\left.\begin{aligned} Q_1 &= \bar{\rho}^{-1}\{\partial_\alpha^2(\partial_t S_3 - gS_4) - \partial_3\partial_\alpha(\partial_t S_\alpha + f\epsilon_{\alpha\beta}S_\beta)\}, \\ Q_2 &= \bar{\rho}^{-1}\{\partial_\alpha^2(\partial_t S_6 + g\bar{\rho}S_5) - \partial_\alpha(\partial_t S_\alpha + f\epsilon_{\alpha\beta}S_\beta)\}, \\ Q_3 &= S_7. \end{aligned}\right\} \tag{2.13}$$

As the forcing functions Q_j depend on all field components, (2.10) and (2.11) are not closed. Their advantage becomes obvious when dealing with weak-interaction problems. The lowest-order fields are then obtained from the linearized equations of motion, and the response may conveniently be calculated from (2.10) and (2.11). Also the response to external forcing may be obtained as any of the S_j may be identified with an external forcing field, e.g. the atmospheric pressure (S_6) or an imposed displacement at the surface (S_5).

If $Q_j = 0$ ($j = 1, 2, 3$) the solution of (2.10) with boundary conditions (2.11) may be represented as a superposition of linear free gravity waves:†

$$u_3(\mathbf{x}, z, t) = \sum_{\mathbf{k},\lambda} A_{\mathbf{k}}^{\lambda} \phi_{\mathbf{k}}^{\lambda}(z) \exp[i(\mathbf{k}\,.\,\mathbf{x} - \omega_{\mathbf{k}}^{\lambda} t] + \text{c.c.} \tag{2.14}$$

with arbitrary amplitudes $A_{\mathbf{k}}^{\lambda}$. The (real) vertical normal mode $\phi_{\mathbf{k}}^{\lambda}(z)$ is the solution of the eigenvalue problem

$$\left.\begin{aligned} \frac{1}{\bar{\rho}}(\bar{\rho}\phi')' + k^2 \frac{N^2 - \omega^2}{\omega^2 - f^2}\,\phi &= 0, \\ \phi' - \frac{gk^2}{\omega^2 - f^2}\,\phi &= 0 \quad \text{at} \quad x_3 = 0, \\ \phi &= 0 \quad \text{at} \quad x_3 = -H, \end{aligned}\right\} \tag{2.15}$$

with eigenvalue $\omega^2 = (\omega_{\mathbf{k}}^{\lambda})^2$. This eigenvalue problem yields the surface gravity wave mode $\lambda = g$ and an infinite set of internal gravity wave modes $\lambda = 1, 2, \ldots$ for which ω is confined between f and the maximum stability frequency.

† We shall use $z = x_3$ and use a prime to denote d/dz. $\mathbf{x}$ and $\mathbf{k}$ are horizontal vectors.

From (2.15) we find the orthogonality relation

$$\int_{-H}^{0} dz\bar{\rho}(N^2-f^2)\,\phi_{\mathbf{k}}^{\lambda}\phi_{\mathbf{k}}^{\mu}+g\bar{\rho}\phi_{\mathbf{k}}^{\lambda}\phi_{\mathbf{k}}^{\mu}|_{z=0}=\delta_{\lambda\mu}((\omega_{\mathbf{k}}^{\lambda})^2-f^2). \tag{2.16}$$

The normalization has been chosen in order to simplify the notation for the total wave energy [see (3.8)].

The response in the internal wave mode λ due to the forcing Q_j is derived by evaluating

$$\int_{-H}^{0} dz\,\bar{\rho}\phi_{\mathbf{k}}^{\lambda}(\mathscr{L}[u_3])_{\mathbf{k}}=\int_{-H}^{0} dz\,\bar{\rho}\phi_{\mathbf{k}}^{\lambda}Q_{1\mathbf{k}}. \tag{2.17}$$

Using the eigenvalue equation (2.15) and the boundary conditions (2.11), the left-hand side reduces to

$$\int_{-H}^{0} dz\,\bar{\rho}\phi_{\mathbf{k}}^{\lambda}(\mathscr{L}[u_3])_{\mathbf{k}}=\bar{\rho}\phi_{\mathbf{k}}^{\lambda}Q_{2\mathbf{k}}|_{z=0}+\bar{\rho}(\phi_{\mathbf{k}}^{\lambda})'\,[\partial_t^2+f^2]\,Q_{2\mathbf{k}}|_{z=-H} - k^2\{\ddot{a}_{\mathbf{k}}^{\lambda}+(\omega_{\mathbf{k}}^{\lambda})^2 a_{\mathbf{k}}^{\lambda}\}, \tag{2.18}$$

where $a_{\mathbf{k}}^{\lambda}(t)$ is the projection of the response

$$u_3(\mathbf{x},z,t)=\sum_{\mathbf{k}} u_{3\mathbf{k}}(z,t)\,e^{i\mathbf{k}.\mathbf{x}} \tag{2.19}$$

on the mode λ, i.e.

$$a_{\mathbf{k}}^{\lambda}=\frac{1}{(\omega_{\mathbf{k}}^{\lambda})^2-f^2}\left\{\int_{-H}^{0} dz\bar{\rho}(N^2-f^2)\,\phi_{\mathbf{k}}^{\lambda}u_{3\mathbf{k}}+g\bar{\rho}\phi_{\mathbf{k}}^{\lambda}u_{3\mathbf{k}}|_{z=0}\right\}. \tag{2.20}$$

According to (2.17) and (2.18) these modal amplitudes satisfy

$$\ddot{a}_{\mathbf{k}}^{\lambda}+(\omega_{\mathbf{k}}^{\lambda})^2 a_{\mathbf{k}}^{\lambda}=\frac{1}{k^2}\left\{-\int_{-H}^{0} dz\bar{\rho}\phi_{\mathbf{k}}^{\lambda}Q_{1\mathbf{k}}+\bar{\rho}\phi_{\mathbf{k}}^{\lambda}Q_{2\mathbf{k}}|_{z=0}+\bar{\rho}(\phi_{\mathbf{k}}^{\lambda})'\,[\partial_t^2+f^2]\,Q_{3\mathbf{k}}|_{z=-H}\right\}. \tag{2.21}$$

The structure of Q_1 and Q_2 allow simplification of the forcing term in this equation by partial integration. This yields

$$\ddot{a}_{\mathbf{k}}^{\lambda}+(\omega_{\mathbf{k}}^{\lambda})^2 a_{\mathbf{k}}^{\lambda}=\frac{1}{k^2}\left\{\int_{-H}^{0} dz\,[(\phi_{\mathbf{k}}^{\lambda})'\,\tilde{Q}_{2\mathbf{k}}-\phi_{\mathbf{k}}^{\lambda}\hat{Q}_{1\mathbf{k}}] + \phi_{\mathbf{k}}^{\lambda}\hat{Q}_{2\mathbf{k}}|_{z=0}+\bar{\rho}(\phi_{\mathbf{k}}^{\lambda})'\,[\partial_t^2+f^2]\,Q_{3\mathbf{k}}|_{z=-H}\right\}, \tag{2.22}$$

where

$$\left.\begin{aligned}\hat{Q}_1&=\partial_\alpha^2[\partial_t S_3-gS_4],\\ \hat{Q}_2&=\partial_\alpha^2[\partial_t S_6+\bar{\rho}gS_5],\\ \tilde{Q}_2&=-\partial_\alpha[\partial_t S_\alpha+f\epsilon_{\alpha\beta}S_\beta].\end{aligned}\right\} \tag{2.23}$$

Equation (2.21) or (2.22) may be used to obtain the internal wave response to any forcing which can be cast into the form of the S_j.

3. The spectral transfer equation

The structure of the linear wave field is obtained by solving the homogeneous linearized equations of motion (2.2) and boundary conditions (2.5) and (2.8). This yields the familiar free-wave solutions with a vertical normal-mode structure:

$$\begin{pmatrix} u_\alpha \\ u_3 \\ \rho \\ p \\ \zeta \end{pmatrix} = \sum_\lambda \frac{A_\lambda}{\omega_\lambda k^2} \begin{pmatrix} (i\omega_\lambda k_\alpha - f\epsilon_{\alpha\beta}k_\beta)\, d/dz \\ \omega_\lambda k^2 \\ -ik^2\bar{\rho}' \\ i\bar{\rho}(\omega_\lambda^2 - f^2)\, d/dz \\ ik^2 \end{pmatrix} \phi_\lambda(z) \exp\{i(\mathbf{k}\,.\,\mathbf{x} - \omega_\lambda t)\}. \tag{3.1}$$

We have simplified the notation by using the subscript λ for $(\lambda, \mathbf{k})$. Reality of the fields is achieved by introducing negative mode numbers and defining

$$A_{-\lambda} = A_\lambda^*, \quad \omega_{-\lambda} = -\omega_\lambda, \quad \phi_{-\lambda} = \phi_\lambda, \tag{3.2}$$

where $-\lambda$ is an abbreviation for $(-\lambda, -\mathbf{k})$. The summation is always over positive and negative mode numbers as well as over all wave vectors $\mathbf{k}$ (generally a continuum).

The lowest-order response due to the presence of the linear wave field (3.1) is obtained by evaluating the Q_j correct to the second order in the linear wave amplitudes. The structure of the result

$$\ddot{a}_\lambda + \omega_\lambda^2 a_\lambda = \sum_{\mu,\nu} A_\mu A_\nu D_{-\lambda\mu\nu} \exp\{-i(\omega_\mu + \omega_\nu)t\} \tag{3.3}$$

can easily be perceived. Here we use $\mu = (\mu, \mathbf{k}_\mu)$ and $\nu = (\nu, \mathbf{k}_\nu)$. The coupling coefficient $D_{-\lambda\mu\nu}$ is given in appendix A. It is symmetric in μ and ν. Note that by construction $D_{-\lambda\mu\nu}$ is defined only for positive mode numbers λ. If we use the convention that it is independent of the sign of the mode number λ, then

$$D_{-\lambda,-\mu,-\nu} = D_{\lambda\mu\nu}^*. \tag{3.4}$$

Equation (3.3) is the familiar evolution equation for the amplitudes of interacting wave triads. It has been frequently discussed in the literature (e.g. Hasselmann 1966; Phillips 1974). Also, the derivation of the spectral transfer for a weakly interacting stochastic quasi-Gaussian ensemble of waves has been demonstrated in various papers (e.g. Hasselmann 1966, 1967; Davidson 1967). The random-phase approximation yields the spectral transfer equation

$$\frac{d}{dt} F_\lambda = \sum_{\mu,\nu} T_{-\lambda\mu\nu}\, \omega_\lambda \{\omega_\lambda F_\mu F_\nu - \omega_\mu F_\lambda F_\nu - \omega_\nu F_\lambda F_\mu\}, \tag{3.5}$$

which describes the rate of change of the spectrum of the λth mode

$$F_\lambda = 2\langle A_\lambda A_{-\lambda}\rangle. \tag{3.6}$$

The angle brackets denote the ensemble average. Conservation of the wave energy has been assumed to derive the scattering integral in the form (3.5), which involves only one scattering cross-section

$$T_{\lambda\mu\nu} = \frac{\pi}{\omega_\lambda^2} |D_{\lambda\mu\nu}|^2\, \delta(\mathbf{k} + \mathbf{k}_\mu + \mathbf{k}_\nu)\, \delta(\omega_\lambda + \omega_\mu + \omega_\nu). \tag{3.7}$$

This is an *a priori* result when working in a Lagrangian framework (Hasselmann 1966, 1967), where the coupling coefficients are inherently completely symmetric and the conservation theorems may be deduced.

The normalization (2.17) of the vertical modes has been chosen such that F_λ is the spectrum of the total wave energy per unit surface area:

$$\frac{1}{2}\left\langle \int_{-H}^{0} dz\,\bar{\rho}(u_j^2 + N^2\zeta^2) + \bar{\rho}g\zeta^2|_{z=0} \right\rangle = \sum_\lambda \langle A_\lambda A_{-\lambda}\rangle = \sum_{\lambda>0} \int d^2k F^\lambda(\mathbf{k}). \tag{3.8}$$

In the last identity we have switched to a continuous representation of the spectrum by defining

$$F^\lambda(\mathbf{k}) = F_\lambda/(\Delta k)^2, \tag{3.9}$$

where Δk is the wavenumber increment in the Fourier sums used so far. For our goal of investigating the transfer from the surface gravity wave field to the internal wave modes we need only the first term in the curly bracket of (3.5). Sorting out the terms with $\mu, \nu = \pm g$, we find that the transfer is

$$\begin{aligned} S^\lambda(\mathbf{k}) = \omega^2 \int d^2k_1 \int d^2k_2 F^g(\mathbf{k}_1) F^g(\mathbf{k}_2) \\ \times \{\delta(\mathbf{k}_1 + \mathbf{k}_2 - \mathbf{k})\,\delta(\omega_1 + \omega_2 - \omega)\,T_{-\lambda\mu\nu} \\ + 2\delta(\mathbf{k}_1 - \mathbf{k}_2 - \mathbf{k})\,\delta(\omega_1 - \omega_2 - \omega)\,T_{-\lambda\mu-\nu}\}, \end{aligned} \tag{3.10}$$

where $\mu = (g, \mathbf{k}_1)$ and $\nu = (g, \mathbf{k}_2)$. Here and in the following analysis we only use positive frequencies; thus $\omega = \omega_\lambda$, $\omega_1 = \omega_\mu$ and $\omega_2 = \omega_\nu$ are the positive internal and surface wave frequencies, respectively. The transfer rate $S^\lambda(\mathbf{k})$ describes the initial rate of change of the internal wave spectrum in the absence of internal waves, i.e. with initial conditions $F^\lambda(\mathbf{k}, t = 0) = 0$. If internal waves are excited $S^\lambda(\mathbf{k})$ still gives the transfer from the surface waves to the internal waves, but to describe the entire coupling between the fields all terms in (3.5) with either μ or ν equal to $\pm g$ must be considered.

The first term in the curly brackets of (3.10) scarcely contributes to $S^\lambda(\mathbf{k})$ taking observed spectral distributions of surface wave energy. The surface wave frequencies are much larger than $N_{\max}$, so that the resonance condition $\omega_1 + \omega_2 = \omega$ cannot be satisfied. Therefore the energy transfer from the surface gravity wave field to the λth internal wave mode reduces to

$$S^\lambda(\mathbf{k}) = \int d^2k_1 F^g(\mathbf{k}_1) F^g(\mathbf{k}_1 - \mathbf{k})\,T\,\delta(\omega_1 - \omega_2 - \omega) \tag{3.11}$$

with

$$T = (2\pi/\omega^2)\,|D^{-\lambda, g, -g}_{-\mathbf{k}, \mathbf{k}_1, \mathbf{k}-\mathbf{k}_1}|^2. \tag{3.12}$$

In the ocean the surface wave energy is located within a frequency range which is separated by at least an order of magnitude from the frequency band of internal waves, i.e. we have $\omega_j \gg \omega$. Unless ω comes close to the maximum stability frequency we also have $k_j \gg k$ and conclude from the resonance conditions

$$\omega = \omega_1 - \omega_2, \quad \mathbf{k} = \mathbf{k}_1 - \mathbf{k}_2 \tag{3.13}$$

that the interacting surface wave components must propagate almost parallel to each other. A more detailed analysis of the resonance conditions follows in the next section.

The transfer rate $S^\lambda(\mathbf{k})$ describes the change in the total energy per unit surface area. Changes in the local quantities can be obtained from the representation (3.1).

For instance, the local transfer rate for potential and horizontal kinetic energy are related to $S^{\nu}(\mathbf{k})$ by

$$S^{\lambda}_{\text{pot}}(\mathbf{k}, z) = \tfrac{1}{2}\bar{\rho}(z)\, N^2(z)\, (\phi_\lambda(z)/\omega_\lambda)^2\, S^{\lambda}(\mathbf{k}) \tag{3.14}$$

and

$$S^{\lambda}_{\text{kin}}(\mathbf{k}, z) = \tfrac{1}{2}\bar{\rho}(z)\, (k^{-1}\phi'_\lambda)^2\, S^{\lambda}(\mathbf{k}) \tag{3.15}$$

respectively.

4. The spectral transfer in a deep ocean

In this paper we shall discuss the spectral transfer for only rather simple models of the stratification and the surface wave spectrum. The aim is to establish the basic structure and magnitude of the transfer and its dependence on the basic parameters of the models. Results for observed stratifications and spectra will be considered in a separate paper. Moreover we restrict ourselves to surface waves in a deep ocean (i.e. $k_j H \gg 1, j = 1, 2$), where the surface wave mode and eigenfrequency are given by

$$\phi_g(z) = (k/\rho_0)^{\frac{1}{2}}\, e^{kz}, \quad \omega_g = (gk)^{\frac{1}{2}}. \tag{4.1}$$

The mode has been normalized in accordance with (2.16) and (3.8) and ρ_0 is the density at the surface.

It is convenient to transform (3.11) to horizontal polar co-ordinates (k, ψ) and eliminate the δ-function. This yields a form which is suitable for analytical and numerical treatment:

$$S^{\lambda}(k, \psi) = \sum_{\text{sgn}\,(\psi - \psi_1)} \int_{k_{1\min}}^{k_{1\max}} dk_1 F^{g}(k_1, \psi_1)\, F^{g}(k_2, \psi_2)\, T\, \frac{k}{k_2} \left| \frac{d\omega_2}{d\psi_1} \right|^{-1}. \tag{4.2}$$

The quantities with subscript 2 can be eliminated by means of (3.13), which yields

$$\left.\begin{aligned} k_2 &= (k^2 + k_1^2 - 2kk_1 \cos\gamma)^{\frac{1}{2}}, \\ \psi_2 &= \psi - (\alpha + \gamma)\, \text{sgn}\,(\psi - \psi_1), \\ \alpha &= \arcsin\{(k/k_2) \sin\gamma\} \end{aligned}\right\} \tag{4.3}$$

and

$$\cos\gamma = \frac{1}{2}\left\{ \frac{k_1}{k} + \frac{k}{k_1} - \frac{[\omega - (gk_1)^{\frac{1}{2}}]^4}{g^2 k k_1} \right\}, \tag{4.4}$$

where α is the angle between $\mathbf{k}_1$ and $\mathbf{k}_2$ and γ the angle between $\mathbf{k}$ and $\mathbf{k}_1$. The function $\cos\gamma$ is shown in figure 1 for various values of $\Omega = \omega/(gk)^{\frac{1}{2}}$ (for oceanic conditions Ω is always small compared with 1). Resonance is possible (i.e. $|\cos\gamma| \leqslant 1$) in the interval $k_{1\min} \leqslant k_1 \leqslant k_{1\max}$ where

$$\left.\begin{aligned} k_{1\min} &= \tfrac{1}{2}k\{1 + \Omega(2 - \Omega^2)^{\frac{1}{2}}\}, \\ k_{1\max} &= k\left(\frac{1 + \Omega^2}{2\Omega}\right)^2. \end{aligned}\right\} \tag{4.5}$$

Figure 2 gives a schematic representation of the possible resonant triplets $\mathbf{k}_1$, $\mathbf{k}_2$ and $\mathbf{k}$.

The integrand in (4.2) becomes singular at the integration limits since

$$\left| \frac{d\omega_2}{d\psi_1} \right|^{-1} = \frac{2(\omega_1 - \omega)^3}{g^2 k k_1 \sin\gamma}. \tag{4.6}$$

These (integrable) singularities pose no serious problem since for reasonable conditions the surface wave energy is confined to wavenumbers k_g with $k_{1\min} \ll k_g \ll k_{1\max}$. For numerical evaluation the singularities can be separated and treated analytically.

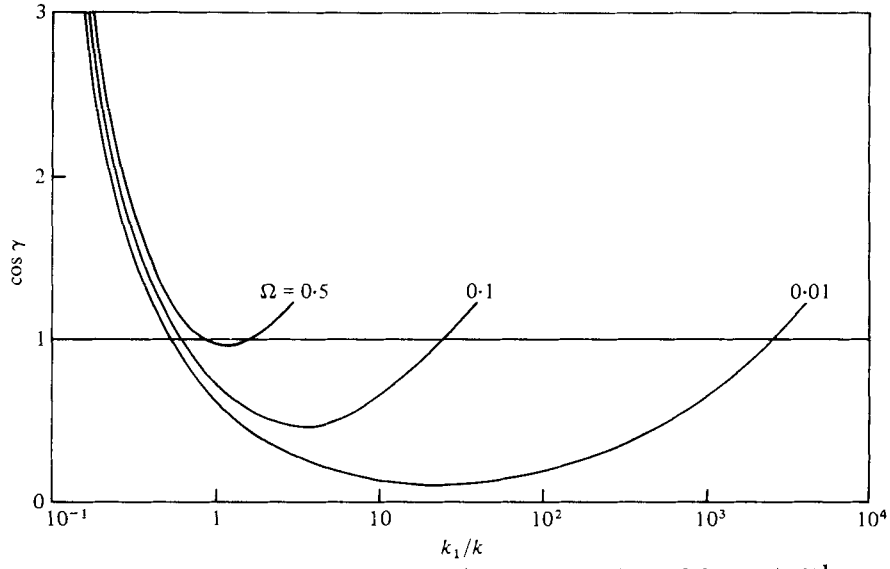

FIGURE 1. cos γ as a function of k_1/k for some values of $\Omega = \omega/(gk)^{\frac{1}{2}}$.

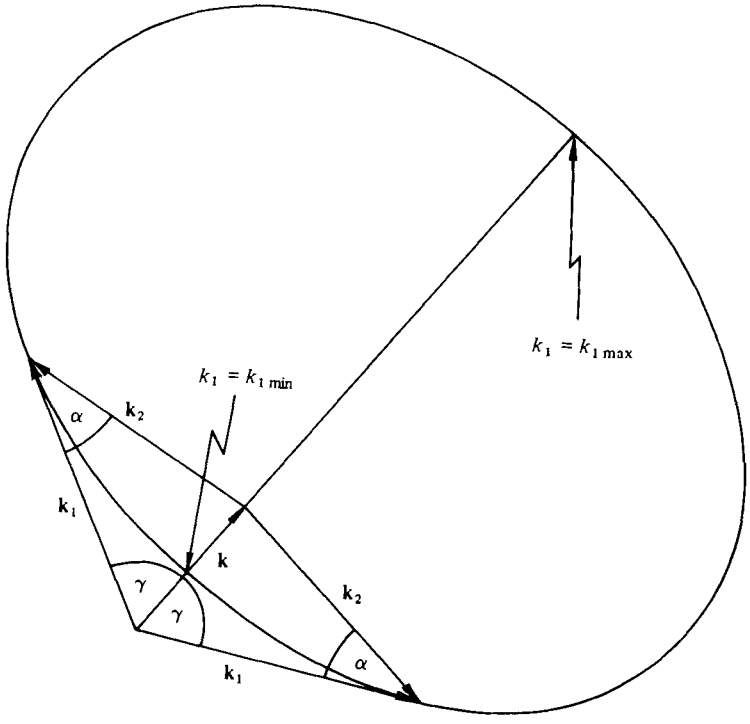

FIGURE 2. Schematic graph of the resonance curve. If $|\cos\gamma| \leqslant 1$ there are two resonant triplets for each $\mathbf{k}$.

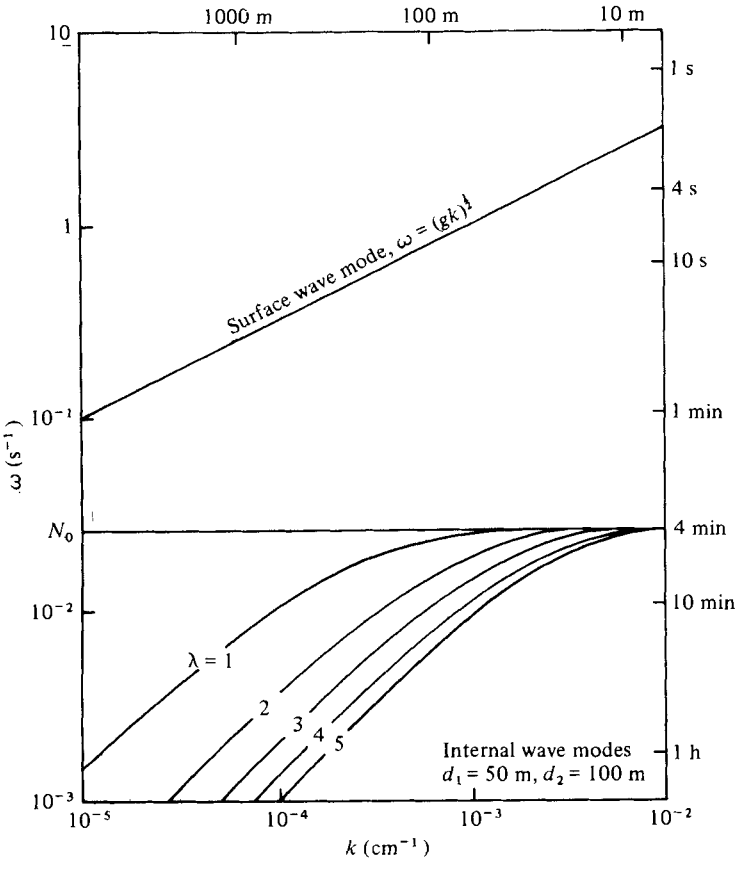

FIGURE 3. Dispersion relations of the surface wave mode and the internal wave modes in a seasonal thermocline.

For surface waves in deep water the transfer function (3.12) simplifies greatly because of the simple structure of ϕ_g and ω_g. We find

$$T = 2\pi(1+\cos\alpha)^2 \left| \rho_0 \phi_\lambda \phi_\mu \phi_\nu|_{z=0} + \int_{-H}^{0} dz \bar{\rho} \frac{N^2}{g} \phi_\lambda \phi_\mu \phi_\nu \right|^2, \tag{4.7}$$

where $\mu = (g, \mathbf{k}_1)$ and $\nu = (g, \mathbf{k}_2)$.

4.1. *Models and basic parameters*

As a model for the stability frequency $N(z)$ we take a simple box

$$N(z) = \begin{cases} N_0 & \text{for} \quad -d_1 \geqslant z \geqslant -d_2, \\ 0 & \text{otherwise.} \end{cases} \tag{4.8}$$

The internal wave modes are then sinusoidal inside the box and exponentially decreasing towards the surface $z = 0$ and the bottom $z = -H$ (for details see appendix B). This model has the advantage that the transfer function (4.7) can be evaluated analytically. Moreover, the parameters N_0, d_1 and d_2 can be adjusted to model either a main thermocline or a seasonal thermocline in the ocean. The model is able to represent

only one of these thermoclines at a time, but this is not a serious restriction since the energy is transferred mainly to high frequency internal waves (i.e. to frequencies around $\frac{1}{2}N_0$). The internal wave modes at these high frequencies of the main thermocline are almost unaffected by a thin seasonal thermocline. This applies also to high frequency modes in the seasonal thermocline if $\frac{1}{2}N_0$ and the maximum stability frequency in the main thermocline are well separated. Since the energy transfer is concentrated at high frequencies ($\omega \gg f$) we shall for simplicity neglect the rotation. Figure 3 shows the dispersion relation for internal waves for the box model of $N(z)$ with parameters appropriate to a seasonal thermocline. Included is the relation (4.1) for the surface wave mode.

It is convenient to represent the surface wave spectrum in the form

$$F^g(k, \psi) = E(k)\, A(\psi, k), \tag{4.9}$$

where the directional distribution (spreading function) $A(\psi, k)$ at each wavenumber is normalized to one. Then $E(k)$ is the wavenumber spectrum of the total energy:

$$E = \rho_0 g \langle \zeta^2 \rangle = \int_0^\infty dk\, E(k). \tag{4.10}$$

It will be demonstrated below that the transfer rate depends only on some basic parameters of the wavenumber distribution $E(k)$. These are the scale parameters (total wave energy E, and peak wavenumber k_m) and the (scaled) bandwidth $2\sigma_E$ of the spectrum, which will be defined such that its product with the mean energy level yields the total energy, i.e.

$$2\sigma_E k_m \int_0^\infty dk\, \frac{E(k)}{E}\, E(k) = E,$$

or

$$2\sigma_E = \frac{1}{k_m} \left(\int_0^\infty dk\, E(k) \right)^2 \Big/ \int_0^\infty dk\, E^2(k). \tag{4.11}$$

Other shape parameters are comparatively unimportant.

The shape of the directional distribution has a strong influence on the shape of $S^\lambda(k, \psi)$. However, it will be shown that the wavenumber distribution of the transfer rate,

$$S^\lambda(k) = \int_0^{2\pi} d\psi\, S^\lambda(k, \psi), \tag{4.12}$$

and the total transfer rate, i.e.

$$S^\lambda = \int_0^\infty dk\, S^\lambda(k), \tag{4.13}$$

again depend only on the bandwidth

$$2\sigma_A(k) = \frac{1}{2\pi} \left\{ \int_0^{2\pi} d\psi\, A^2(\psi, k) \right\}^{-1} \tag{4.14}$$

of $A(\psi, k)$ and not significantly on any other shape parameter.

These properties enable us to discuss the transfer integral and derive a parametrization of $S^\lambda(k, \psi)$ and its integrals (4.12) and (4.13) without specifying the surface wave spectrum in more detail. The analytical discussion in the next section applies to rather general spectra $E(k)$ as long as they decay rapidly enough and a dominant wavenumber scale k_m can be defined. Also the spreading function is arbitrary. For numerical computations we use completely factorized models, i.e. $A(\psi, k) = A(\psi)$,

and assume that the distributions $E(k)$ and $A(\psi)$ are both smooth functions with a single peak at $k = k_m$ and $\psi = 0$, respectively. This model class allows one to represent one-peaked wind–sea or swell spectra but excludes, for example, a superposition of wind–sea and swell or different swell beams.

4.2. *Parametrization of the transfer integral*

The insensitivity of the transfer rate to the details of the shape of the spectrum $E(k)$ is due to the great difference in the scales of the internal waves and interacting surface wave components. Only closely neighbouring spectral components in the surface wave spectrum interact, so that the transfer integral (4.2) loses its property of being a convolution of the spectrum with itself. Each contribution to $S^\lambda(k,\psi)$ of interacting pairs is rather weighted by the square of the local spectral level. Since the transfer function (4.7) and the Jacobian (4.6) vary slowly compared with the spectrum (if $k_{1\min} \ll (1 \pm \sigma_E) k_m \ll k_{1\max}$) the convolution approximately reduces to an integral of the spectrum squared, which is completely determined by the bandwidth. These considerations will be pursued to establish a parametrization of the transfer rate by the basic parameters of the spectrum and the stratification.

Expanding the transfer integral (4.2) with respect to the ratio of internal and surface wave frequencies (or formally with respect to $\Omega = \omega/(gk)^{\frac{1}{2}} \ll 1$) and the ratio of the wavenumbers ($k/k_m \ll 1$), we obtain to lowest order

$$S^\lambda(k,\psi) = 16\pi E^2 \left(\frac{k_m}{g}\right)^{\frac{1}{2}} \int_0^\infty dx\, x^{\frac{3}{2}}\, G^2(x)\, H^\lambda(x,k) \sum_{s=\pm} A^2(\psi + \tfrac{1}{2}s\pi, xk_m). \tag{4.15}$$

The wavenumber distribution has been expressed as

$$E(k) = (E/k_m)\, G(k/k_m), \tag{4.16}$$

where $G(x)$ is normalized to 1. By taking the upper limit as infinite we have to assume that the spectrum decreases fast enough so that the integral converges. The function

$$H^\lambda(x,k) = \left| \phi_\lambda(0) + \int_0^\infty dz\, \frac{N^2(z)}{g}\, \phi_\lambda(z) \exp(2k_m x z) \right|^2 \tag{4.17}$$

is a remainder of the transfer function (4.7). This is an $O(\Omega^4)$ quantity which expresses the weak coupling between the fields.

The derivation of (4.15) requires not only $\Omega \ll 1$ and $k/k_m \ll 1$ but also $k_m \ll k_{1\max}$, or equivalently, $4\Omega^2 \ll k/k_m$. If $4\Omega^2$ and k/k_m are of the same order of magnitude we get $\sum_s A^2(\psi + s\pi)$ as the angular distribution and $k/(4\Omega^2 k_m)$ as the upper integration limit. Then the transfer rate will strongly depend on the shape of the spectrum. This situation, however, occurs only if the spectral peak is at rather small wavelengths. Such spectra generally have only small energy and the transfer will be negligible.

If $H^\lambda(x,k)$ and $A(\psi, xk_m)$ vary only slowly compared with $G(x)$ we may approximate the transfer rate by

$$S^\lambda(k,\psi) \approx 16\pi E^2 \left(\frac{k_m}{g}\right)^{\frac{1}{2}} H^\lambda(1,k) \sum_{s=\pm} A^2(\psi + \tfrac{1}{2}s\pi, k_m) \int_0^\infty dx\, x^{\frac{3}{2}}\, G^2(x). \tag{4.18}$$

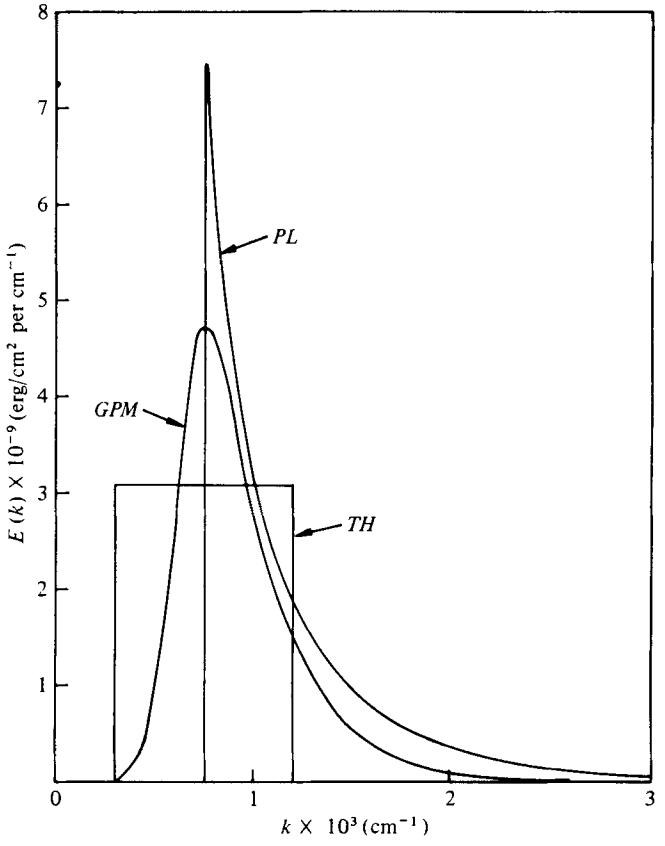

FIGURE 4. Three models of the surface wave spectrum with $2\sigma_E = 1{\cdot}2$. Analytical representation given in appendix C. Spectral parameters given in appendix D.

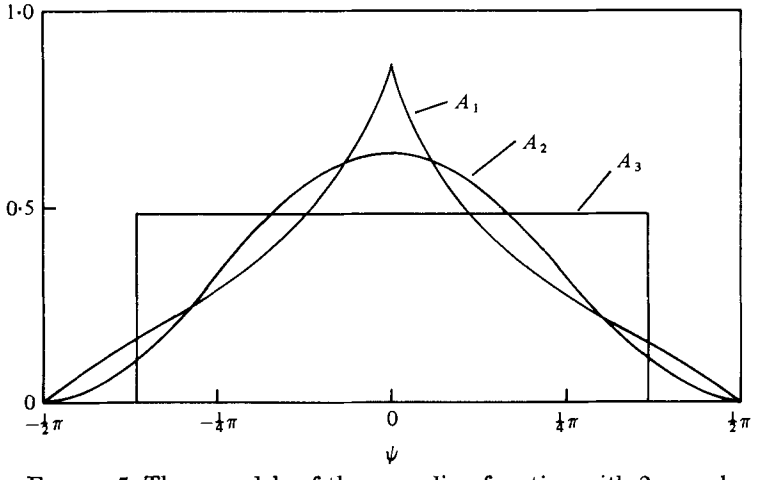

FIGURE 5. Three models of the spreading function with $2\sigma_A = \frac{1}{3}$.

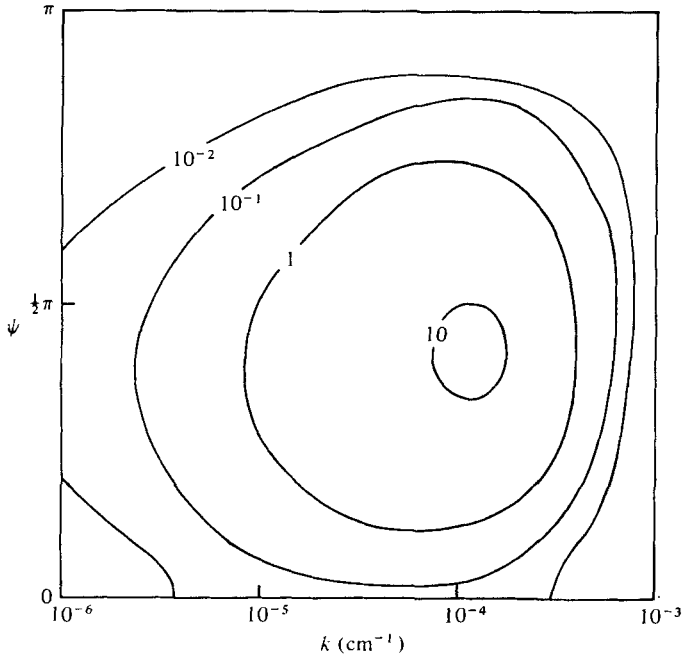

FIGURE 6. Contour of $S^1(k, \psi)$ computed for the combination PL–A_2 and a seasonal thermocline. Units are ergs/cm² s per cm^{-1} rad. Spectral and stratification parameters given in appendix D.

This expression reflects the insensitivity of $S^\lambda(k, \psi)$ to the details of shape of the spectrum since

$$\int_0^\infty dx\, x^{\frac{3}{2}} G^2(x) \approx \int_0^\infty dx\, G^2(x) = \frac{1}{2\sigma_E} \tag{4.19}$$

if $G(x)$ decays rapidly enough away from the peak (cf. appendix C).

The wavenumber distribution $S^\lambda(k)$ may be derived without specifying $A(\psi, k)$. From (4.15) and the definition of σ_A we find

$$S^\lambda(k) = 16\pi E^2 \left(\frac{k_m}{g}\right)^{\frac{1}{2}} \int_0^\infty dx\, \frac{x^{\frac{3}{2}} G^2(x)}{\sigma_A(xk_m)}\, H^\lambda(x, k), \tag{4.20}$$

which turns out to be insensitive to the details of the directional distribution except the bandwidth σ_A. These approximations and the resulting statements about the insensitivity of the transfer rate to the shape of the spectrum have been confirmed by numerical evaluation of the transfer integral (4.2). Figure 4 shows three models of $E(k)$ with same E, k_m and σ_E but different shapes, and figure 5 shows three models of $A(\psi)$ with same bandwidth σ_A (in the half-plane $\frac{1}{2}\pi < \psi < \frac{3}{2}\pi$ all models of $A(\psi)$ are zero). Figure 6 is a contour plot of $S^1(k, \psi)$ computed for the power-law model PL combined with the directional distribution $A_2(\psi)$. Since $S^\lambda(k, \psi)$ is symmetric with respect to the mean propagation direction $\psi = 0$ of the surface wave field, the figures display only the contours for $0 \leqslant \psi \leqslant \pi$. Results for the models PM and TH differ from PL by less than 10%. Figure 7 displays $S^\lambda(k)$ for PL and A_2; the results for the two other directional distributions differ by less than 1%.

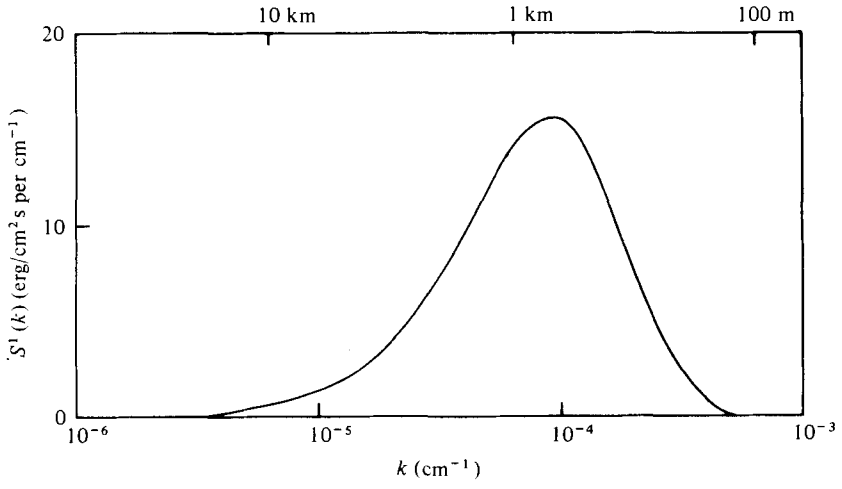

FIGURE 7. Wavenumber distribution $S^1(k)$ of the transfer shown in figure 6.

In the following analysis we shall discuss (4.15) with a stratification given by the box model (4.8). The function $H^\lambda(x,k)$ becomes

$$H^\lambda(x,k) = \left| \phi_\lambda(0) + \left(\frac{N_0}{2\omega_m}\right)^2 \left\{ \frac{\exp(2k_m xz)}{x^2+b^2} \cdot \left[x\phi_\lambda(z) - \frac{1}{k_m}\phi'_\lambda(z) \right] \right\}_{z=-d_1}^{z=-d_2} \right|^2, \quad (4.21)$$

where $b = \beta/(2k_m)$ and $\beta = \beta^\lambda(k)$ is the vertical wavenumber of the λth internal wave mode (see appendix B). We shall take the spectrum to be completely factorized, i.e. $A(\psi,k) = A(\psi)$. Then the transfer rate $S^\lambda(k,\psi)$ is also factorized. The directional dependence turns out to be independent of the wavenumber spectrum $E(k)$ and even independent of the form and scales of the internal wave guide. Internal waves are predominantly generated with wave vectors which are perpendicular to the mean propagation of the surface wave field (cf. also figure 6). This feature has already been found by Kenyon (1968). It is also supported by satellite pictures by Apel *et al.* (1975) showing a wavelike pattern which propagates nearly at right angles to the much shorter wind waves. If $A(\psi)$ is of the form indicated in figure 5 each of the two lobes of $S^\lambda(k,\psi)$ at $\psi = \frac{1}{2}\pi$ and $\psi = -\frac{1}{2}\pi$ is narrower than the generating surface wave beam since generally $\sigma_{A^2} \leqslant \sigma_A$.

The integral (4.15) may be evaluated analytically for an $N(z)$ = constant model (i.e. $d_1 = 0$, $d_2 = H$) and a model of a thin thermocline (i.e. $(d_2 - d_1)\beta \ll 1$) since for these cases the dispersion relation of the internal waves can be expressed analytically (see appendix B).

The case $N(z)$ = constant has been studied by Kenyon (1968). From (4.15) and (4.21) we find

$$S^\lambda(k,\psi) = CJ^\lambda(k)\, I(b) \sum_{s=\pm} A^2(\psi + \tfrac{1}{2}s\pi), \quad (4.22)$$

where

$$C = \omega_m E k_m^2 \langle \zeta^2 \rangle (N_0/\omega_m)^4. \quad (4.23)$$

The wavenumber dependence is given by

$$J^\lambda(k) = \frac{32\pi}{H} \frac{\beta^2 k^2}{(\beta^2+k^2)^3} \quad (4.24)$$

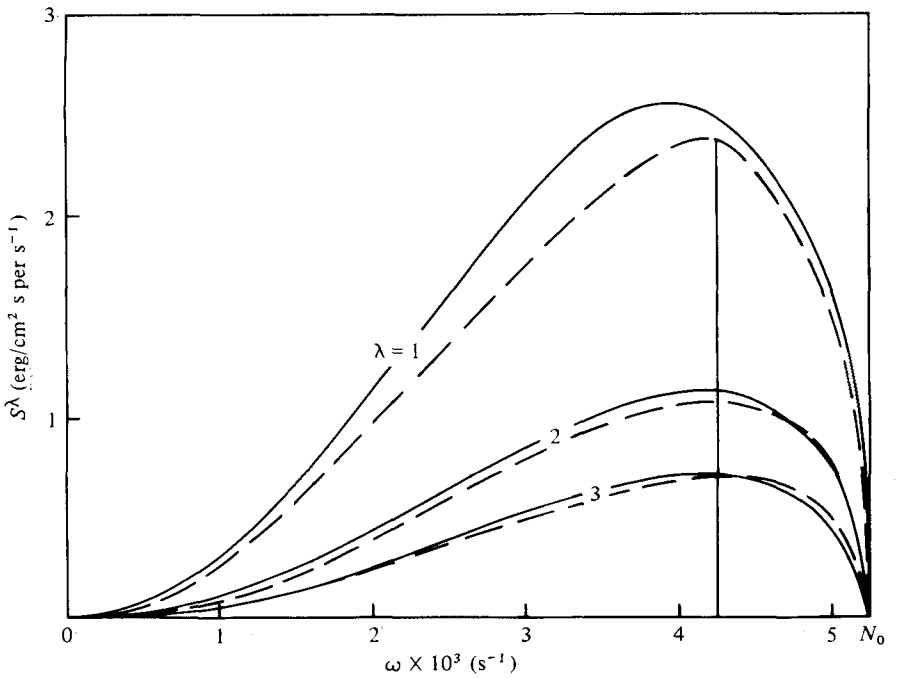

FIGURE 8. Frequency distribution $S^\lambda(\omega)$ of the transfer to an ocean with constant $N = 5{\cdot}25 \times 10^{-3}$ s^{-1} (3 c.p.h.). ——, numerical integration of (4.2); ---, approximation (4.27), (4.28).

since the remaining integral

$$I(b) = \int_0^\infty dx\, x^{\frac{3}{2}} G^2(x) \left(\frac{x^2}{x^2+b^2}\right)^2 \tag{4.25}$$

affects only the modal distribution of the transfer (for constant $N(z)$ the parameter $b = \lambda\pi/(2k_m H)$ does not depend on k). The integral $I(b)$ is evaluated in appendix C for the spectral models shown in figure 5. For low modes $b \ll 1$ and

$$I(b) \approx I(0) \approx 1/2\sigma_E. \tag{4.26}$$

For high modes ($\lambda \gg 2k_m H/\pi$) the integral decreases strongly with mode number, which assures the convergence of the total transfer $\sum_\lambda S^\lambda$ to the internal wave field [see (4.30)]. The transfer rate $S^\lambda(k, \psi)$ and also the wavenumber density

$$S^\lambda(k) = CJ^\lambda(k) I(b)/\sigma_A \tag{4.27}$$

increase quadratically with k towards a peak at $\beta/2^{\frac{1}{2}} = \lambda\pi/2^{\frac{1}{2}}H$ and then drop to zero like k^{-4}. The distribution of the transfer in the frequency domain, $S^\lambda(\omega)$, is obtained by replacing $J^\lambda(k)$ in (4.27) by

$$J^\lambda(\omega) = \left|\frac{d\omega_\lambda}{dk}\right| J^\lambda(k) = \frac{\omega^2(N_0^2-\omega^2)^{\frac{1}{2}}}{\lambda\pi N_0^4}, \tag{4.28}$$

which has a maximum at $(\frac{2}{3})^{\frac{1}{2}} N_0$. Thus high frequency waves with wavelengths of order H/λ are excited. To demonstrate the accuracy of the analytical approximation figure 8 shows the frequency distribution [i.e. (4.27) and (4.28)] for the lowest three modes together with the results of the numerical integration of (4.2).

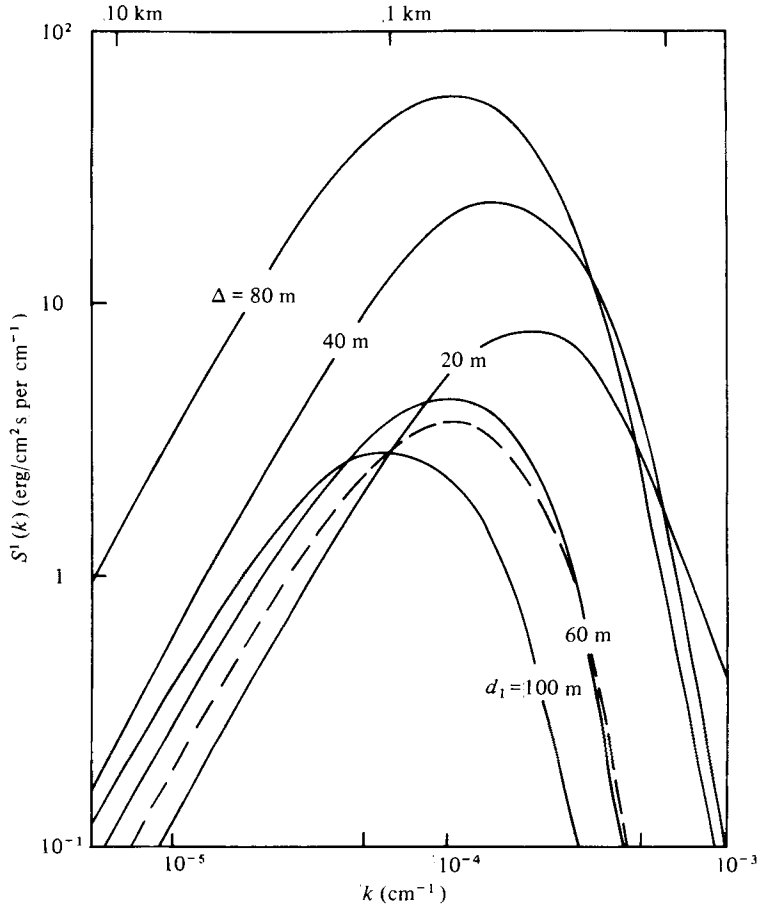

FIGURE 9. Wavenumber distribution $S^1(k)$ of the transfer to a seasonal thermocline for various values of d_1 and Δ. ——, numerical integration; – – –, analytical approximation. The upper three solid curves have $d_1 = 20$ m and variable Δ; the lower three solid curves have $\Delta = 20$ m and variable d_1. The dashed curve has $d_1 = 60$ m, $\Delta = 20$ m. Spectral parameters are given in appendix D.

The total transfer to the λth mode in an ocean with constant stability frequency may be written in the form

$$S^\lambda = \omega_m E/t^\lambda, \tag{4.29}$$

where t^λ is the dimensionless time scale

$$t^\lambda = \lambda \frac{2\sigma_E \sigma_A}{k_m^2 \langle \zeta^2 \rangle} \left(\frac{\omega_m}{N_0}\right)^4 \times \begin{cases} 1 & \text{for} \quad \lambda \ll 2k_m H/\pi, \\ (\lambda\pi/2k_m H)^r & \text{for} \quad \lambda \gg 2k_m H/\pi. \end{cases} \tag{4.30}$$

The exponent r depends on the asymptotic behaviour of $G(x)$ [see (C 2)]. The expression (4.30) indicates that the transfer will be more important the smaller the ratio of surface and internal wave frequency scales, the larger the total energy and average slope of the surface wave field and the sharper the wavenumber and angular distributions. Predominantly low modes are excited. Notice that t^λ/ω_m is the time scale of energy loss of the surface wave field due to the transfer. A characteristic time scale for the internal wave energy E^λ in the λth mode may be defined by E^λ/S^λ.

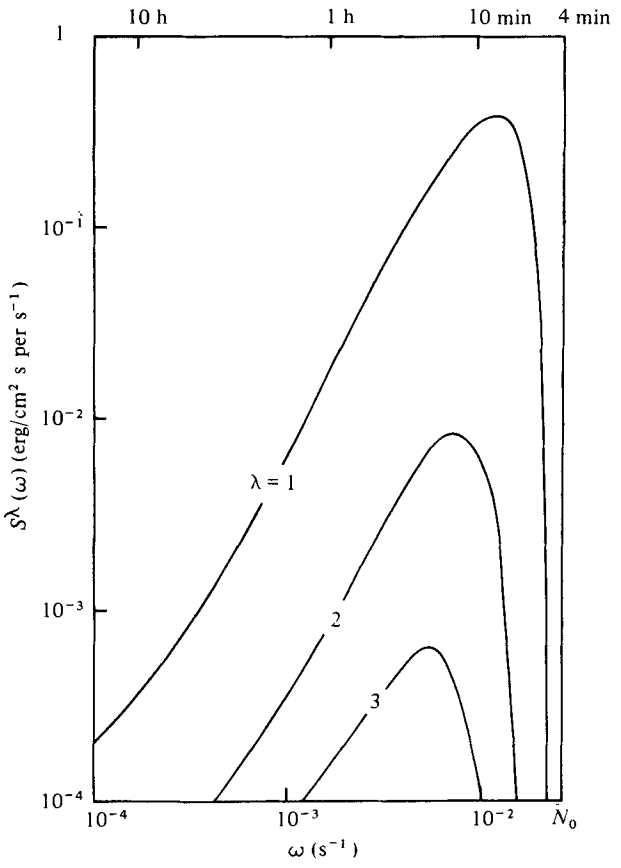

FIGURE 10. Frequency distribution $S^\lambda(\omega)$ of the transfer to a seasonal thermocline. Spectral and stratification parameters given in appendix D.

To understand the dependence of the transfer on the depth d_1 and thickness

$$\Delta = d_2 - d_1$$

of the thermocline we consider the opposite case of a thin thermocline. We may neglect the second term in (4.21) and $H^\lambda(x,k) = \phi_\lambda^2(0)$ can be computed from (B 10) for the first mode. The transfer rate is of the same form (4.22) with $b = 0$ and $J^1(k)$ replaced by

$$\hat{J}^1(k) = 16\pi\Delta \frac{k\Delta \sinh kd_1}{[\exp(kd_1) + k\Delta \sinh kd_1]^3}, \tag{4.31}$$

which also increases quadratically at low wavenumbers but drops exponentially at high wavenumbers. Figure 9 displays numerical computations of $S^1(k)$ for various values of d_1 and Δ. The dominant wavelength decreases with increasing d_1 or Δ and is of the order of 1 km. The frequency structure is shown in figure 10. As for the $N(z)$ = constant model, high frequency waves are generated but a much stronger decrease of the transfer with mode number is obtained (see also figure 12). If $\Delta \ll d_1$, we can give an analytical expression for the dimensionless time scale:

$$\hat{t}^1 = \omega_m E/S^1 = \frac{2\sigma_E\sigma_A}{k_m^2\langle\zeta^2\rangle}\left(\frac{\omega_m}{N_0}\right)^4\left(\frac{d_1}{\Delta}\right)^2. \tag{4.32}$$

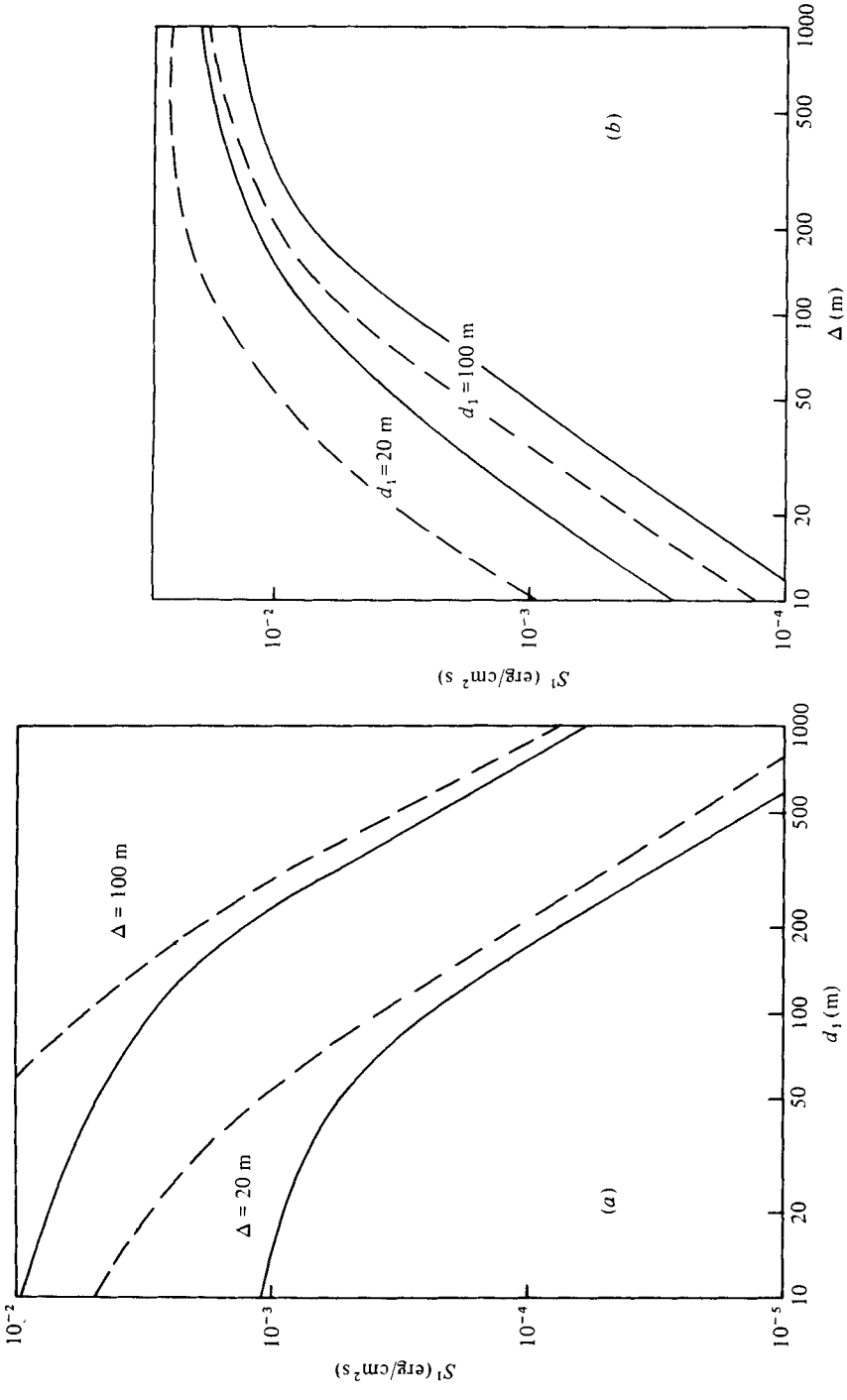

FIGURE 11. Dependence of the transfer rate S^1 on (*a*) the thermocline depth d_1 and (*b*) the thermocline thickness Δ. Spectral parameters given in appendix D. ——, $k_m = 3{\cdot}4 \times 10^{-4}$ cm^{-1}; – – –, $k_m = 7{\cdot}6 \times 10^{-4}$ cm^{-1}.

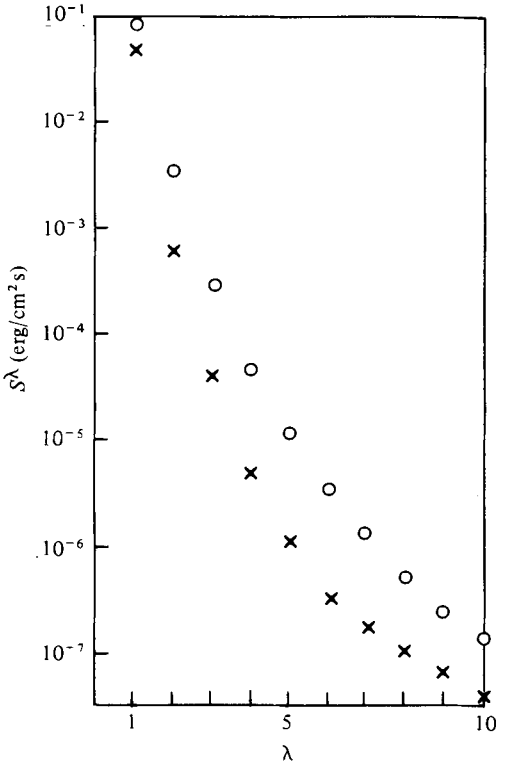

FIGURE 12. Modal dependence of the transfer rate S^λ to a seasonal thermocline. Spectral parameters given in appendix D. ○, $d_1 = 25$ m; ×, $d_1 = 50$ m. $\Delta = 50$ m.

The transfer is thus most important for shallow thermoclines. Comparison of (4.30) and (4.32) shows that the transfer to a thin thermocline is smaller by a factor

$$(\Delta/d_1)^2 \ll 1$$

than the transfer to a water column with constant stratification (and the same N_0).

The parametrizations derived above have been confirmed by numerical integration of the complete transfer integral (4.2), e.g. as demonstrated in figures 8 and 9. The transfer in thermoclines with a shape intermediate between the cases considered so far has been studied numerically. We found that the dependence on N_0 and the spectral parameters is satisfactorily described by the parametrization (4.30) and (4.32). The dependence on the thermocline depth d_1 and thickness Δ is displayed in figure 11 for spectra with same total energy E and different peak wavenumbers k_m. Figure 12 shows the dependence of the total transfer on the mode number λ for two thermocline depths. Compared with the results (4.30) for $N(z) =$ constant, where $S^\lambda \propto 1/\lambda$, the dominance of the first mode in the internal wave response is considerably enlarged.

For wind-sea spectra, i.e. spectra which develop under the action of the local wind, the parametrization may be expressed in terms of the local wind speed and the fetch. The scale parameters k_m and E of the Pierson–Moskowitz (1964) spectrum,

$$E_{\mathrm{PM}}(k) = \frac{E}{k_m}\frac{5}{2}\left(\frac{k}{k_m}\right)^{-3}\exp\left[-\frac{5}{4}\left(\frac{k}{k_m}\right)^{-2}\right], \tag{4.33}$$

depend on the wind speed U as

$$k_m = \omega_m^2/g \propto U^{-2}, \quad E = \rho_0 g \frac{a}{5k_m^2} \propto U^4, \tag{4.34}$$

where $a = 0{\cdot}0081$ is Phillips' constant. These relations imply that

$$S^\lambda \propto \omega_m E^2 \propto U^7. \tag{4.35}$$

The PM-spectrum is a model for a fully developed wind–sea. This form of the spectrum applies to the final stages of development (Hasselmann *et al.* 1976). It is therefore only rarely found in field data. A parametrization of developing spectra leads to the JONSWAP form (Hasselmann *et al.* 1973, 1976)

$$E_J(k) = \tfrac{1}{2}\rho_0 g a k^{-3} \exp\left[-\frac{5}{4}\left(\frac{k}{k_m}\right)^{-2} + \ln c \exp\left\{-\frac{1}{2\sigma^2}\left(\left(\frac{k}{k_m}\right)^{\frac{1}{2}} - 1\right)^2\right\}\right], \tag{4.36}$$

where $\sigma = \sigma_a$ for $k < k_m$ and $\sigma = \sigma_b$ for $k > k_m$. In addition to the scale parameters k_m and a this function contains the three shape parameters c, σ_a and σ_b. Following Hasselmann *et al.* (1973), the fetch dependence of the non-dimensional peak frequency $\omega_* = U\omega_m/g$ and energy $E_* = \rho_0 g^3 E/U^4$ is described by

$$\omega_* = 2\pi \times 3{\cdot}5\xi^{-\frac{1}{3}}, \quad E_* = 1{\cdot}6 \times 10^{-7}\xi, \tag{4.37}$$

where $\xi = gx/U^2$ is the non-dimensional fetch and x the actual fetch. The shape parameters exhibit appreciable scatter but no significant mean dependence on the fetch. The transfer rate then is related to fetch and wind speed by

$$S^\lambda \propto (U^4 E_*)^2 \omega_*/U \propto U^7 \xi^{\frac{5}{3}}. \tag{4.38}$$

These considerations are not valid for swell spectra which are decoupled from the local wind.

The relations (4.29), (4.30) and (4.32) reveal strong dependence of the transfer rate on some model parameters, in particular the surface wave energy or r.m.s. displacement and the frequency ratio of surface and internal waves. (The quadratic increase of the transfer with the surface wave energy is of course a trivial result.) Further parametrizations such as (4.35) and (4.38) which apply to wind–sea spectra suggest a very strong dependence on the local wind speed. We therefore anticipate a large spatial and temporal variability of the transfer. If the process is important at all (which is examined in the next section) this variability and also the specific directionality should help to detect the interaction among other processes in the field data.

4.3. *Magnitude of the transfer*

We shall now evaluate the transfer rate for typical values of the parameters and demonstrate the relevance or irrelevance of the process. Because of the invariance of the transfer to the shape of $E(k)$ (with the exception of σ_E) wind–sea and swell spectra need not be considered separately. We take the JONSWAP spectrum (4.36) combined with the spreading function

$$A_2(\psi) = \frac{1}{\pi}\frac{(2p)!!}{(2p-1)!!}\begin{cases}\cos^{2p}\psi & \text{for } |\psi| \leqslant \tfrac{1}{2}\pi, \\ 0 & \text{otherwise,}\end{cases} \tag{4.39}$$

	$N_0/2\pi$ (c.p.h.)	d_1 (m)	Δ (m)	S^λ (erg/cm² s) $\lambda = 1$	$\lambda = 2$	$\lambda = 3$
N = constant	1	0	5000	$3{\cdot}1 \times 10^{-6}$	$1{\cdot}5 \times 10^{-6}$	$1{\cdot}9 \times 10^{-6}$
Main thermocline	3	100	900	$3{\cdot}2 \times 10^{-4}$	$8{\cdot}4 \times 10^{-5}$	$3{\cdot}1 \times 10^{-5}$
	3	500	500	$7{\cdot}3 \times 10^{-5}$	$1{\cdot}2 \times 10^{-5}$	$8{\cdot}1 \times 10^{-8}$
Seasonal thermocline	15	25	50	$5{\cdot}7 \times 10^{-2}$	$1{\cdot}4 \times 10^{-3}$	$8{\cdot}4 \times 10^{-5}$
		50	50	$3{\cdot}7 \times 10^{-2}$	$4{\cdot}2 \times 10^{-4}$	$2{\cdot}1 \times 10^{-5}$
	20	25	50	$1{\cdot}8 \times 10^{-1}$	$4{\cdot}3 \times 10^{-3}$	$2{\cdot}7 \times 10^{-4}$
		50	50	$1{\cdot}2 \times 10^{-1}$	$1{\cdot}3 \times 10^{-3}$	$6{\cdot}7 \times 10^{-5}$

TABLE 1. The transfer rate S^λ ($\lambda = 1, 2, 3$) for some models of the stratification. A surface wave spectrum with $\langle\zeta^2\rangle = 1$ m² and $2\sigma_E = 0{\cdot}6$, $2\sigma_A = 0{\cdot}33$ was used.

with $p = 1$, which yields $2\sigma_A = \frac{1}{3}$. This distribution is displayed in figure 5. As typical values of the shape parameters of $E_J(k)$ we consider the mean JONSWAP values

$$c = 3{\cdot}3, \quad \sigma_a = 0{\cdot}07, \quad \sigma_b = 0{\cdot}09,$$

which yield a bandwidth $2\sigma_E = 1{\cdot}2$. These values agree with the mean shape parameters of 333 spectra which are representative of the wind–sea climate in the Atlantic and the North Sea (cf. Hasselmann *et al.* 1976). Swell in general has smaller bandwidths σ_E and σ_A.

As scale parameters of the wavenumber spectrum we choose $\langle\zeta^2\rangle = 1$ m² ($E = 9{\cdot}81 \times 10^6$ erg/cm²) and $\omega_m/2\pi = 0{\cdot}1$ Hz (corresponding to a wavelength of 156 m). Transfer rates for other values of $\langle\zeta^2\rangle$ and ω_m follow from $S^\nu \propto \omega_m \langle\zeta^2\rangle^2$. An r.m.s. displacement $\langle\zeta^2\rangle^{\frac{1}{2}} = 1$ m may be regarded as typical for the northern Atlantic. According to the wave statistics of Neu (1976) the significant wave height H_s ($\approx 4\langle\zeta^2\rangle^{\frac{1}{2}}$) exceeds 4 m about 20–30 % of the time and 2 m about 70–80 % of the time at latitudes above 50°. Towards the equator H_s becomes considerably smaller: $H_s > 4$ m about 3 % and $H_s > 2$ m about 40 % of the time.

Table 1 summarizes the results for three cases of the stratification: an ocean with constant $N(z) = N_0$, models of a main thermocline and models of a seasonal thermocline. The ocean depth is $H = 5000$ m. The table mirrors the results of the last section: a strong decrease of S^λ with mode number λ and thermocline thickness Δ and an increase with N_0. The transfer to the seasonal thermocline turns out to be considerably larger than that to the main thermocline. This is due to the stronger stratification (larger N_0) in the seasonal thermocline and the smaller depth d_1 of the mixed layer. The transfer rates to the wave field in the main thermocline are in strong contrast to the recent results of Watson *et al.* (1976), who obtained growth rates of the order of some erg/cm² s. As pointed out in the introduction, this discrepancy is due to the difference in the conception of the spectrum. In our calculations we have modelled the spectrum by a random ensemble of wave components while Watson *et al.* used a finite set of deterministic waves. Generally a wave which is subject to resonant forcing grows much faster if driven by a deterministic field than if driven by a stochastic field since in the latter case the optimum phase relation for energy exchange between the forcing field component and growing wave component will be destroyed by phase-mixing of the spectral components which support the wave. The time scale $t^\lambda/\omega_m = E/S^\lambda$ is larger than 1 year even for the largest S^λ in table 1, i.e. the surface

wave field does not feel the energy loss. To estimate the importance of the transfer for the internal wave field we have to evaluate the characteristic time scale E^λ/S^λ for the energy E^λ in the λth internal wave mode.

The wave field in the main thermocline can be described by an universal, quasi-stationary spectrum. The energy is spread over many modes. According to the GM-model (Garrett & Munk 1975) and the IWEX-model (Müller, Olbers & Willebrand 1977) E^λ is of order 10^5 erg/cm^2 for the first ten or so modes, so that $E^1/S^1 \approx 3 \times 10^8$ s $\sim$ 10 years. If we consider that the process generates high frequency waves only we get a smaller time scale. The energy E^λ_{hf} in the high frequency part (say $\omega > \frac{1}{2}N$) of the internal wave spectrum is of order $E^\lambda f/N$. This yields

$$E^1_{hf}/S^1 \approx 1 \text{ month}.$$

Characteristic time scales of other processes affecting the main thermocline wave field are of the order of several periods (cf. Müller & Olbers 1975). In the high frequency region we frequently find time scales that are even less than a period, e.g. the time scale for nonlinear interactions within the wave field (Olbers 1976; McComas & Bretherton 1977). Thus the process is completely unimportant for internal waves in the main thermocline.

Internal waves which are trapped in the seasonal thermocline show quite different properties from the main thermocline wave field. These high frequency waves occur (frequently as bursts of distinct wave groups) intermittently in space and time (Sabinin 1973). The energy is predominantly in the first mode (Brekhovskikh *et al.* 1975). The slope of the spectrum at high frequencies shows a large variability. Frequently there is a broad peak or plateau in the spectrum well before the stability frequency, e.g. in the GATE-spectra (Käse & Clarke 1978). The local energy in the high frequency part of the spectrum is typically of order 1–5 erg/cm^3, which vertically integrates to about 10^4 erg/cm^2. This yields a characteristic time scale

$$E^1/S^1 \approx 1 \text{ day}$$

for the response in the first mode. Referring to the parametrization (4.32) of the transfer rate, we must conclude that in extreme situations the surface wave field is able to generate high frequency waves very efficiently in the seasonal thermocline, e.g. for $\langle\zeta^2\rangle = 2$ m^2, $\sigma_A = \sigma_E = \frac{1}{2}$ yields $E^1/S^1 \approx 0{\cdot}1$ day. But even in rather calm situations the process may play an important role if there is a strong stratification. The coarse agreement of the modal decomposition of the transfer (cf. figure 10) with observations might be evidence for the occurrence of the interaction. However, other processes, e.g. resonant generation of internal waves by wind-stress fluctuations, show a similar modal dependence (Käse 1979; see also §5). Also, the burst-like occurrence of high frequency waves in the seasonal thermocline can be explained by the onset of storms or the intersecting of swell beams. For such cases there will be a sudden increase of the transfer rate because of the strong dependence on the wind speed or surface wave energy.

5. Summary and conclusions

The spectral energy transfer from surface to internal waves has been studied to establish its importance in the ocean. The spectral transfer equation and the coupling coefficients have been derived in a general form by weak-interaction theory. The

further discussion was restricted to surface waves in deep water and to a simple three-layer model of the stability frequency: a thermocline with constant stability frequency and homogeneous top and bottom layers. This is still a reasonable model since the process generates high frequency waves whose modal structure is almost unaffected by the details of the stratification outside the thermocline. The wavenumber distribution of the surface wave spectrum did not need to be specified in more detail than by its scales and its bandwidth since the transfer rate turned out to be insensitive to the shape of the spectrum with the exception of the bandwidth. For this reason a distinction between swell and wind–sea is not necessary. Numerical evaluations of the transfer rate were performed using the spectral models of Pierson & Moskowitz (1964), JONSWAP (Hasselmann *et al.* 1973) or simpler ones, combined with spreading functions which are symmetric about a dominant propagation direction. Analytical results have been derived for arbitrary spreading functions. The insensitivity of the transfer to the shape of the spectrum could be attributed to the great difference in the scales of the interacting fields. Only close neighbours in the spectrum can satisfy the resonance conditions. This feature has been exploited to derive a parametrization of the transfer integral in terms of the basic parameters of the stratification and the spectrum. For wind–sea spectra the parametrization can be carried further by introducing phenomenological relations between the spectral scales and the local wind speed. A strong dependence of the transfer on some model parameters is revealed, in particular the ratio of internal and surface frequency scales, the significant wave height, and the local wind speed. The transfer rate therefore has a large variability in space and time even if the ranges of relevant parameters are narrow (e.g. doubling the wind speed increases the transfer by two orders of magnitude).

For the parameter regime of oceanic main thermoclines the transfer is negligibly small. Assuming that our stochastic model is applicable to the ocean surface wave field in the mean, this process must definitely be excluded from the list of possible candidates for maintaining the internal wave field in the main thermocline. In some situations a deterministic model such as the one of Watson *et al.* (1976) may be a more realistic description of the sea state (e.g. in the case of long swell waves). Then the transfer may locally be larger but the process still does not contribute to the overall energy balance of the ocean internal wave field.

The frequency gap between surface waves and internal waves which are trapped in the seasonal thermocline is smaller than the gap between surface waves and internal waves in the main thermocline. The coupling to the seasonal thermocline is therefore considerably stronger. For moderate surface wave conditions we find characteristic transfer times of the order of a day. In extreme situations such as strong storms or crossing swell components of high amplitude the time scale will be a fraction of a day. Concerning global variability, the process is presumably most effective in higher latitudes. The transfer indeed decreases with the thermocline depth, which is larger at high latitudes, but the rougher surface wave field in this region will dominate this effect.

The process shows some outstanding features which may help it to be observed in the field data and distinguished from other processes which generate internal waves in the seasonal thermocline. The response is predominantly in the first mode at high frequencies, and the horizontal wavelengths are of order 1 km. The wave vectors of the internal waves generated are nearly perpendicular to those of the surface waves,

so that for collimated beams of surface waves we shall find a characteristic directional pattern in the response. Finally, the response will have a marked intermittent structure in space and time because of the strong parametric dependence of the transfer rate. Most observations of high frequency waves in the seasonal thermocline show these properties. This, however, is not sufficient evidence for the process since many properties are shared by competitive processes, e.g. resonant generation of internal waves by atmospheric pressure or wind-stress fluctuations. The reason becomes obvious on rewriting the approximation (4.15) made for the seasonal thermocline in the form

$$S^{\lambda}(k,\psi) = \pi|\phi_{\lambda}(0)|^2 \frac{8E^2\omega_m}{g\sigma_E} \sum_{s=\pm} A^2(\psi + \tfrac{1}{2}s\pi). \tag{5.1}$$

This expression shows that the modal and wavenumber (or frequency) dependence is exclusively determined by the waveguide and not by the external forcing field, which determines only the directional distribution and the magnitude of the transfer rate. Consider now the resonant response to atmospheric pressure fluctuations described by a spectral transfer rate

$$S_p^{\lambda}(k,\psi) = \pi|\phi_{\lambda}(0)|^2 F_p(k,\psi,\omega=\omega_{\lambda}), \tag{5.2}$$

or to wind-stress fluctuations with

$$S_{\tau}^{\lambda}(k,\psi) = \pi|\phi_{\lambda}(0)|^2 (gk/\omega_{\lambda}^2)^2 F_{\tau}(k,\psi,\omega=\omega_{\lambda}). \tag{5.3}$$

These transfer rates may be derived from the internal wave response equation (2.22). The modal and wavenumber dependence of these functions closely resembles (5.1). If the pressure spectrum $F_p(k,\psi,\omega)$ and the wind-stress spectrum $F_{\tau}(k,\psi,\omega)$ are flat in the resonance region the three transfer rates will indeed be distinguishable only by their magnitudes and directional distributions (at high frequencies ω^2/gk varies only slightly, cf. figure 3). Insufficient knowledge of the wavenumber and frequency structure of the spectra F_p and F_{τ} at present prevents a detailed theoretical analysis of (5.2) and (5.3) in the high frequency region (the low frequency response has been treated by Käse 1979). The problem of the relevance of the different transfer mechanisms can be solved by correlating time variations of the response, i.e. parameters of the internal wave spectrum, with the different surface forcing. This is one of the aims of the JASIN-experiment.

This research was supported by the Deutsche Forschungsgemeinschaft and is a contribution of the Sonderforschungbereich 94, Meersforschung, Hamburg. Helpful discussions with Dr Rolf Käse and Dr Dieter Hasselmann are gratefully acknowledged.

Appendix A. The coupling coefficient for wave–wave interactions

General expression

The coupling coefficient $D_{-\lambda\mu\nu}$ is obtained by inserting the linear solutions (3.1) into the source terms S_j (correct to second order in the wave amplitude as defined in § 2) and evaluating the forcing term of the internal wave response equation. This yields an expression of the form

$$\sum_{\mu,\nu} A_{\mu} A_{\nu} G_{-\lambda\mu\nu} \exp\{-i(\omega_{\mu}+\omega_{\nu})t\}$$

with an asymmetrical coefficient $G_{-\lambda\mu\nu}$. The symmetrical (in the last two indices) coupling coefficient is then given by

$$D_{-\lambda\mu\nu} = \tfrac{1}{2}\{G_{-\lambda\mu\nu} + G_{-\lambda\nu\mu}\}. \tag{A 1}$$

Explicitly we find (for $f = 0$)

$$D_{-\lambda\mu\nu} = \tfrac{1}{2}i(\omega_\mu + \omega_\nu)\left\{\int_{-H}^{0} dz\,\bar{\rho}N^2(R_{-\lambda\mu\nu}\phi_\lambda + S_{-\lambda\mu\nu}\phi'_\lambda) + \rho_0 T_{-\lambda\mu\nu}\phi_\lambda|_{z=0}\right\} \tag{A 2}$$

with

$$\begin{aligned}
R_{-\lambda\mu\nu} &= \frac{1}{g}\left(\frac{\omega_\mu^2+\omega_\nu^2}{\omega_\mu\omega_\nu}+1\right)\phi_\mu\phi_\nu + \frac{2}{g}\frac{\mathbf{k}_\mu\cdot\mathbf{k}_\nu}{k_\mu^2 k_\nu^2}\phi'_\mu\phi'_\nu \\
&\quad - \left[\frac{\mathbf{k}_\mu\cdot\mathbf{k}_\nu}{k_\mu^2\omega_\nu^2}\phi'_\mu\phi_\nu + \frac{1}{\omega_\mu+\omega_\nu}\left(\frac{\mathbf{k}_\mu\cdot\mathbf{k}_\nu}{k_\mu^2}+1\right)\frac{1}{\omega_\mu}\phi'_\mu\phi_\nu + (\mu\leftrightarrow\nu)\right], \\
S_{-\lambda\mu\nu} &= -\frac{1}{\omega_\mu\omega_\nu}\phi_\mu\phi_\nu + \left[\frac{\omega_\mu+\omega_\nu}{g\omega_\mu}\frac{\mathbf{k}_\lambda\cdot\mathbf{k}_\nu}{k_\lambda^2 k_\nu^2}\phi_\mu\phi'_\nu - \frac{\mathbf{k}_\lambda\cdot\mathbf{k}_\nu}{k_\lambda^2\omega_\nu^2}\phi_\mu\phi_\nu + (\mu\leftrightarrow\nu)\right], \\
T_{-\lambda\mu\nu} &= \frac{\omega_\mu^2+\omega_\nu^2}{\omega_\mu\omega_\nu}\phi_\mu\phi_\nu - \frac{\mathbf{k}_\mu\cdot\mathbf{k}_\nu}{k_\mu^2 k_\nu^2}\phi'_\mu\phi'_\nu + \phi_\mu\phi_\nu \\
&\quad - \frac{g}{\omega_\mu+\omega_\nu}\left[\left(\frac{\mathbf{k}_\mu\cdot\mathbf{k}_\nu}{k_\mu^2}+1\right)\frac{1}{\omega_\nu}\phi'_\mu\phi_\nu + (\mu\leftrightarrow\nu)\right].
\end{aligned} \tag{A 3}$$

The operation of symmetrization has been abbreviated in an obvious manner. The coupling coefficient has been reduced somewhat by partial integration and use of the eigenvalue equations (2.15). A simple correspondence between the surface (T) and volume terms (R and S) in $D_{-\lambda\mu\nu}$ and the surface (S_5, S_6) and volume (S_i, $i = 1, \ldots, 4$) forcing functions is therefore no longer possible.

The coupling coefficient in the form (A 2) still applies to arbitrary modes λ, μ and ν and ocean depth H. The order of magnitude of the various terms and their importance depend strongly on the kind of modes we want to consider. If all three modes are internal waves the volume terms generally dominate since the vertical displacement at the surface due to internal waves is very small.

If μ and ν correspond to surface waves, the case we want to study, surface and volume terms may be of comparable magnitude. This seems to be paradoxical since the surface term seems to vanish if we define the internal wave modes by changing the surface boundary condition of (2.16) to the rigid-lid approximation $\phi_\lambda = 0$ at $z = 0$. However, in this case we have to use a different forcing in the internal wave response equation (2.22) which is similar to that associated with the bottom term. The coupling coefficient then would have a surface term proportional to $\phi'_\lambda(0)$.

Problem of the Boussinesq approximation

There has been some discussion about the use of the Boussinesq approximation in deriving the coupling coefficient, in particular for the case of surface–internal wave interactions (Brekhovskikh *et al.* 1972). The Boussinesq version of $D_{-\lambda\mu\nu}$ is obtained by expansion of (A 2) with respect to $\delta = L_z\bar{\rho}'/\rho_0$, where L_z is the vertical scale of the waves considered and ρ_0 is the average density of the water column. As $L_z \leqslant H$ and $\rho_0/\bar{\rho}' = O(200\text{ km})$ we have $\delta \ll 1$.

If μ and ν are internal wave modes all terms in $D_{-\lambda\mu\nu}$ are $O(1)$ except those which

are proportional to $1/g$. These are $O(\delta)$ and thus negligible. The Boussinesq approximation of the eigenvalue problem (2.16) is

$$\left.\begin{aligned} &\phi'' + k^2 \frac{\hat{N}^2 - \omega^2}{\omega^2}\phi = 0, \\ &\phi' - \frac{gk^2}{\omega^2}\phi = 0 \quad \text{at} \quad z = 0, \\ &\phi = 0 \quad \text{at} \quad z = -H \end{aligned}\right\} \tag{A 4}$$

with $\hat{N}^2 = (-g/\rho_0)\bar{\rho}'$.

If μ and ν are surface waves we find a quite different result. Here $L_z = 1/k_g$ thus

$$\delta = \frac{1}{k_g}\frac{\bar{\rho}'}{\rho_0} = -\frac{\hat{N}^2}{gk_g}, \tag{A 5}$$

so that terms proportional to N^2/ω_g^2 are also $O(\delta)$. This applies to all terms in (A 3) (even the surface term), so that the complete coupling coefficient $D_{-\lambda\mu\nu}$ is $O(\delta)$. The Boussinesq approximation is thus not applicable in this case. The internal wave mode λ, however, may be determined from the Boussinesq version (A 4) and the surface wave mode from the corresponding $O(1)$ eigenvalue problem

$$\left.\begin{aligned} &\phi'' - k^2\phi = 0, \\ &\phi' - \frac{gk^2}{\omega^2}\phi = 0 \quad \text{at} \quad z = 0, \\ &\phi = 0 \quad \text{at} \quad z = -H. \end{aligned}\right\} \tag{A 6}$$

The coupling coefficient $D_{-\lambda\mu\nu}$ is then correct to $O(\delta)$.

Coupling coefficient for surface–internal wave interactions in deep water

The coupling coefficient $D_{-\lambda\mu\nu}$ simplifies greatly for surface waves in deep water. Using $\omega_g^2 = gk$ and $\phi_g' = k\phi_g$, we find that many terms cancel (in particular $S_{-\lambda\mu\nu} = 0$). We obtain

$$D_{-\lambda\mu\nu} = -i(\omega_\mu + \omega_\nu)\left(\frac{\mathbf{k}_\mu \cdot \mathbf{k}_\nu}{k_\mu k_\nu} - 1\right)\left\{\rho_0 \phi_\lambda \phi_\mu \phi_\nu|_{z=0} + \int_{-H}^{0} dz \bar{\rho}\frac{N^2}{g}\phi_\lambda \phi_\mu \phi_\nu\right\}. \tag{A 7}$$

Notice that the coefficient is separated into a geometrical factor depending on the relative orientation of the interacting wave vectors $\mathbf{k}_\mu$ and $\mathbf{k}_\nu$ and a factor which is independent of the geometry. The geometrical dependence implies that for sum interactions (both frequencies positive) the coupling is zero for parallel $\mathbf{k}_\mu$ and $\mathbf{k}_\nu$ while for difference interactions (one frequency negative) the coupling vanishes if the vectors are antiparallel.

Appendix B. Internal wave eigenfunctions

As a basic model for the stability frequency $N(z)$ we choose the box model (4.8). The solution of the eigenvalue problem (A 4) is given by

$$\phi(z) = \left\{\begin{aligned} &AS(kz) \quad \text{for} \quad 0 \geqslant z \geqslant -d_1, \\ &B\sin\beta z + C\cos\beta z \quad \text{for} \quad -d_1 \geqslant z \geqslant -d_2, \\ &D\sinh k(z+H) \quad \text{for} \quad -d_2 \geqslant z \geqslant -H, \end{aligned}\right. \tag{B 1}$$

with

$$\beta = k\left(\frac{N_0^2-\omega^2}{\omega^2}\right)^{\frac{1}{2}} \tag{B 2}$$

and

$$S(x) = \tfrac{1}{2}(e^x - \epsilon e^{-x}). \tag{B 3}$$

The upper boundary condition in (A 4) is satisfied if

$$\epsilon = \frac{1-\omega^2/gk}{1+\omega^2/gk}. \tag{B 4}$$

The rid-lid approximation, i.e. $\phi(0) = 0$, is obtained as the lowest-order term of an expansion with respect to ω^2/gk, which yields $\epsilon = 1$.

The values of A, B, C and D and the dispersion relation are obtained from the normalization condition

$$\rho_0 \frac{N_0^2}{\omega^2}\int_{-d_2}^{-d_1} \phi^2 dz + \frac{\rho_0 g}{\omega^2}\phi^2(0) = 1 \tag{B 5}$$

and the continuity of ϕ and ϕ' at $z = -d_1$ and $z = -d_2$. We find

$$B = \left(\frac{2}{\rho_0(d_2-d_1)}\frac{\omega^2}{N_0^2}\right)^{\frac{1}{2}}\left[1+g^2-\frac{\sin\beta(d_2-d_1)}{\beta(d_2-d_1)}\left\{2y\sin\beta(d_2+d_1)\right.\right.$$
$$\left.\left.+(1-y^2)\cos\beta(d_2+d_1)\right\}\right]+\frac{(1-\epsilon)^2}{2}\frac{g}{N_0^2(d_2-d_1)}\left\{\frac{\sin\beta d_1 - y\cos\beta d_1}{S(-kd_1)}\right\}^2, \tag{B 6a}$$

$$A = B\frac{y\cos\beta d_1 - \sin\beta d_1}{S(-kd_1)}, \quad D = B\frac{y\cos\beta d_2 - \sin\beta d_2}{\sinh k(H-d_2)} \tag{B 6b, c}$$

with

$$y = \frac{C}{B} = \frac{\sin\beta d_2 + (\beta/k)\tanh k(H-d_2)\cos\beta d_2}{\cos\beta d_2 - (\beta/k)\tanh k(H-d_2)\sin\beta d_2}. \tag{B 7}$$

The dispersion relation is

$$\tan\beta(d_2-d_1) = -\frac{\beta}{k}\frac{\tanh k(H-d_2) - T(-kd_1)}{1+(\beta^2/k^2)\tanh k(H-d_2)\,T(-kd_1)} \tag{B 8}$$

with

$$T(x) = (e^x - \epsilon e^{-x})/(e^x + \epsilon e^{-x}). \tag{B 9}$$

There are solutions of (B 8) at discrete values of $\beta = \beta^\lambda(\omega)$, which yield the frequencies $\omega = \omega_k^\lambda$ ($\lambda = 1, 2, \ldots$) of the internal wave modes.

Equation (B 8) is easily solved for a constant stability profile ($d_1 = 0$, $d_2 = H$). To lowest order in ω^2/gk the vertical wavenumber becomes $\beta^\lambda = \lambda\pi/H$. The normalization constant (B 6) is $B = (2/\rho_0 H)^{\frac{1}{2}}\omega/N_0$. Also, the opposite case of a thin thermocline, i.e. $(d_2-d_1)\beta \ll 1$, can be treated analytically (cf. also Phillips 1977, p. 211). We find for the first mode

$$\left.\begin{aligned}\omega^2 &= N_0^2\frac{k\Delta}{1+k\Delta+\coth kd_1},\\ A &= \frac{\omega}{N_0}\frac{1}{(\rho_0\Delta)^{\frac{1}{2}}\sinh kd_1} = -D\frac{\sinh k(H-d_1)}{\sinh kd_1}\end{aligned}\right\} \tag{B 10}$$

with $\Delta = d_2 - d_1$.

Appendix C. Evaluation of the integral $I(b)$

$$I(b) = \int_0^\infty dx\, x^{\frac{3}{2}} G^2(x) \left(\frac{x^2}{x^2+b^2}\right)^2,$$

where $G(x)$ is the normalized surface wave spectrum defined by (4.16). The integral $I(b)$ exists if $G(x)$ decays faster than $x^{-\frac{5}{4}}$. We are particularly interested in the behaviour for $b \ll 1$ (low modes) and $b \gg 1$ (high modes, convergence of the total transfer). We shall evaluate $I(b)$ for three models of $G(x)$ (special cases are displayed in figure 4) and find that for $b \ll 1$

$$I(b) = A(1 - 2Bb^2 + \ldots) \tag{C 1}$$

and for $b \gg 1$

$$I(b) \sim \begin{cases} Cb^{-4} & \text{for } q > \frac{13}{4}, \\ Db^{-2q+\frac{5}{2}} & \text{for } q < \frac{13}{4}, \end{cases} \tag{C 2}$$

if $G(x) \sim x^{-q}$. If $G(x)$ decays fast enough ($q > \frac{13}{4}$) the constants A, B and C become

$$A \approx C \approx 1/2\sigma_E, \quad B \approx 1. \tag{C 3}$$

For all three models $I(b)$ can be expressed in terms of special functions which are tabulated in Abramowitz & Stegun (1964). The integral can be found in Gradshteyn & Ryzhik (1965) if the transformation $\eta = 1/x^2$ is made, which casts $I(b)$ into the form

$$I(b) = \frac{1}{2}\int_0^\infty d\eta\, \frac{\eta^{-\frac{9}{4}}}{(1+\eta b^2)^2}\, G^2(\eta^{-\frac{1}{2}}). \tag{C 4}$$

The results for the three models are as follows.

(*a*) *Top-hat model*

$$G_{\mathrm{TH}}(x) = \begin{cases} 1/2\sigma_E & \text{if } |x-1| < \sigma_E, \\ 0 & \text{otherwise,} \end{cases}$$

$$I_{\mathrm{TH}}(b) = \left[\frac{2}{5}\frac{1}{(2\sigma_E)^2}\, \eta^{-\frac{5}{4}}\, {}_2F_1(2, -\tfrac{5}{4}; -\tfrac{1}{4}; -\eta b^2)\right]_{(1-\sigma_E)^{-2}}^{(1+\sigma_E)^{-2}},$$

$$A = C = 1/2\sigma_E, \quad B = D = 1.$$

(*b*) *Power-law model*

$$G_{\mathrm{PL}}(x) \begin{cases} (q-1)\, x^{-q} & \text{if } x \geqslant 1, \\ 0 & \text{otherwise,} \end{cases}$$

with

$$2\sigma_E = (2q-1)/(q-1)^2,$$

$$I_{\mathrm{PL}}(b) = \frac{1}{2\sigma_E}\, \frac{q-\frac{1}{2}}{q-\frac{5}{4}}\, {}_2F_1(2, q-\tfrac{5}{4}; q-\tfrac{1}{4}; -b^2),$$

$$A = \frac{1}{2\sigma_E}\, \frac{q-\frac{1}{2}}{q-\frac{5}{4}}, \quad B = \frac{q-\frac{5}{4}}{q-\frac{1}{4}},$$

$$C = \frac{1}{2\sigma_E}\, \frac{q-\frac{1}{2}}{q-\frac{13}{4}}, \quad D = A\,\Gamma(q-\tfrac{1}{4})\,\Gamma(\tfrac{13}{4}-q)$$

(*c*) *Generalized Pierson–Moskowitz model.* Notice that for the PM-model (4.33) the spectral peak appears at $(\frac{5}{6})^{\frac{1}{2}} k_m$ [but in the original frequency spectrum at $(gk_m)^{\frac{1}{2}}$].

To obtain a spectrum with variable bandwidth and slope we generalize the PM-spectrum slightly:

$$G_{\mathrm{GPM}}(x) = 2(\tfrac{1}{2}q)^{\frac{1}{2}(q-1)} \frac{x^{-q}}{\Gamma\{\frac{1}{2}(q-1)\}} \exp[-\tfrac{1}{2}qx^{-2}],$$

with $$2\sigma_E = 2^{q-2}q^{\frac{1}{2}}\Gamma^2\{\tfrac{1}{2}(q-1)\}/\Gamma\{\tfrac{1}{2}(2q-1)\}.$$

Then $$I_{\mathrm{GPM}}(b) = 2^{2-q}q^{\frac{1}{2}(q+\frac{1}{2})}\Gamma(q-\tfrac{5}{4})\,\Gamma^{-2}\{\tfrac{1}{2}(q-1)\}\,b^{-q+\frac{1}{4}}\exp[q/(2b^2)]\,W_{\kappa,\lambda}(qb^{-2})$$

with $$\kappa = \tfrac{1}{2}(\tfrac{1}{4}-q), \quad \lambda = \tfrac{1}{2}(q-1\tfrac{3}{4}),$$

$$A = \frac{q^{\frac{3}{4}}}{2\sigma_E}\frac{\Gamma(q-\frac{5}{4})}{\Gamma(q-\frac{1}{2})}, \quad B = \frac{q-\frac{5}{4}}{q}.$$

$$C = \frac{q^{1\frac{1}{4}}}{2\sigma_E}\frac{\Gamma(q-1\frac{3}{4})}{\Gamma(q-\frac{1}{2})}, \quad D = Aq^{q-\frac{5}{4}}\Gamma(1\tfrac{3}{4}-q).$$

In (*a*) and (*b*) ${}_2F_1$ is Gauss' hypergeometric series and in (*c*) $W_{\kappa,\lambda}$ is Whittaker's function.

Appendix D. Model parameters used for the figures

The ocean depth was

$$H = 5000 \text{ m}.$$

The standard model of seasonal thermocline with

$$d_1 = 50 \text{ m}, \quad d_2 = 100 \text{ m}, \quad N_0 = 2{\cdot}6 \times 10^{-2} \text{ s}^{-1} \text{ (15 c.p.h.)}$$

was used in figures 3, 6, 7, 10 and 12.

Models of the surface wave spectrum $E(k)$ are given by (4.33) (PM) and appendix C (TH, PL, GPM). Standard parameters are

$$E = 2{\cdot}79 \times 10^6 \text{ erg/cm}^2, \langle\zeta^2\rangle = (53 \text{ cm})^2,$$

$$k_m = 7{\cdot}6 \times 10^{-4} \text{ cm}^{-1}, \omega_m = 0{\cdot}86 \text{ s}^{-1} \text{ (0·137 Hz)};$$

these were used in figures 4 (PL with $q = 3$, GPM with $q = 7$), 6 and 7 (PL with $q = 3$), and 8–12 (PM). Figure 11 additionally uses PM with $E = 2{\cdot}79 \times 10^6$ erg/cm^2, $k_m = 3{\cdot}4 \times 10^{-4}$ cm^{-1} and $\omega_m = 0{\cdot}59$ s^{-1} (0·092 Hz). The bandwidth of PM is

$$2\sigma_E = \tfrac{8}{3}(5/2\pi)^{\frac{1}{2}} = 2{\cdot}4.$$

For all figures the spreading function (4.39) was used, with $p = 1$ in figures 5–7, $p = 2$ in figure 8 and $p = 3$ in figures 9–12. The bandwidth of A_2 is

$$2\sigma_A = \frac{1}{2\pi}\frac{(4p)!!\,(2p-1)!!}{(4p-1)!!\,(2p)!!}.$$

REFERENCES

ABRAMOWITZ, M. & STEGUN, E. A. (ed.) 1972 *Handbook of Mathematical Functions*. Dover.

APEL, J. R., BYRNE, H. M., PRONI, J. R. & CHARNELL, R. L. 1975 Observations of oceanic internal and surface waves from the earth resources technology satellite. *J. Geophys. Res.* **80**, 865–881.

BALL, F. K. 1964 Energy transfer between external and internal gravity waves. *J. Fluid Mech.* **19**, 465.

BREKHOVSKIKH, L. M., GONCHAROV, V. V., KURTEPOV, V. M. & NAUGOL'NYKH, K. A. 1972 Resonant excitation of internal waves by nonlinear interaction of surface waves. *Izv. Atmos. Ocean. Phys.* **8**, 192–203.

BREKHOVSKIKH, L. M., KONJAEV, K. V., SABININ, K. D. & SERIKOV, A. N. 1975 Short-period internal waves in the sea. *J. Geophys. Res.* **80**, 856–864.

DAVIDSON, R. C. 1967 The evolution of wave correlations in uniformly turbulent, weakly non-linear systems. *J. Plasma Phys.* **1**, 341–359.

GARRETT, C. & MUNK, W. 1975 Space-time scales of internal waves: a progress report. *J. Geophys. Res.* **80**, 291–297.

GRADSHTEYN, I. S. & RYZHIK, I. M. 1965 *Table of Integrals, Series and Products.* Academic Press.

HASSELMANN, K. 1966 Feynman diagrams and interaction rules of wave–wave scattering processes. *Rev. Geophys. Space Phys.* **4**, 1–32.

HASSELMANN, K. 1967 Nonlinear interactions treated by the methods of theoretical physics (with applications to the generation of waves by wind). *Proc. Roy. Soc.* A **299**, 77–100.

HASSELMANN, K. *et al.* 1973 Measurements of wind-wave growth and swell decay during the Joint North Sea Wave Project (JONSWAP). *Dsche Hydr. Z. Suppl.* A(8°) no. 12.

HASSELMANN, K., ROSS, D. B., MÜLLER, P. & SELL, W. 1976 A parametric wave prediction model. *J. Phys. Ocean.* **6**, 200–228.

JOYCE, T. M. 1974 Nonlinear interactions among standing surface and internal gravity waves. *J. Fluid Mech.* **63**, 801–825.

KÄSE, R. 1979 Calculations of the energy transfer by the wind to near-inertial internal waves. *Deep-Sea Res.* In press.

KÄSE, R. & CLARKE, R. A. 1978 High frequency internal waves in the upper thermocline during GATE. *Deep-Sea Res.* **25**, 815–825.

KENYON, K. E. 1968 Wave–wave interactions of surface and internal waves. *J. Mar. Res.* **26**, 208–231.

MCCOMAS, C. H. & BRETHERTON, F. P. 1977 Resonant interaction of oceanic internal waves. *J. Geophys. Res.* **82**, 1397–1412.

MÜLLER, P. & OLBERS, D. J. 1975 On the dynamics of internal waves in the deep ocean. *J. Geophys. Res.* **80**, 3848–3860.

MÜLLER, P., OLBERS, D. J. & WILLEBRAND, J. 1977 The IWEX spectrum. *J. Geophys. Res.* **83**, 479–500.

NESTEROV, S. V. 1972 Resonant interactions of surface and internal waves. *Izv. Atmos. Ocean. Phys.* **8**, 252–254.

NEU, H. J. A. 1976 Wave climate in the North Atlantic – 1970. *Bedford Inst. Oceanog., Rep.* B1-R-76-10.

OLBERS, D. J. 1976 Nonlinear energy transfer and the energy balance of the internal wave field in the deep ocean. *J. Fluid Mech.* **74**, 375–399.

PHILLIPS, O. M. 1977 *The Dynamics of the Upper Ocean.* Cambridge University Press.

PHILLIPS, O. M. 1974 Wave interactions. In *Nonlinear Waves* (ed. S. Leibovich & A. R. Seebass). Cornell University Press.

PIERSON, W. J. & MOSKOWITZ, L. 1964 A proposed spectral form for fully developed wind seas based on the similarity theory of S. A. Kitaigorodskii. *J. Geophys. Res.* **69**, 5181–5190.

SABININ, K. D. 1973 Certain features of short-period internal waves in the ocean. *Izv. Atmos. Ocean. Phys.* **9**, 66–74.

THORPE, S. A. 1966 On wave interactions in a stratified fluid. *J. Fluid Mech.* **24**, 737–751.

WATSON, K. M., WEST, B. J. & COHEN, B. I. 1976 Coupling of surface and internal gravity waves: a mode coupling model. *J. Fluid Mech.* **77**, 185–208.